2013-12-09

# Template-free synthesis and modification of LTY, ZSM-5 and LTL zeolite catalysts and investigation of the catalytic pyrolysis of Saskatchewan boundary dam coal

Motazedi, Kavan

UNIVERSITY OF CALGARY

# Template-free synthesis and modification of LTY, ZSM-5 and LTL zeolite catalysts and investigation of the catalytic pyrolysis of Saskatchewan boundary dam coal

by

Kavan Motazedi

A THESIS

SUBMITTED TO THE FACULTY OF GRADUATE STUDIES

IN PARTIAL FULFILMENT OF THE REQUIREMENTS FOR THE

DEGREE OF MASTER OF SCIENCE

CHEMICAL AND PETROLEUM ENGINEERING

CALGARY, ALBERTA

December, 2013

## Abstract

In this study, new approaches were adopted toward the template-free synthesis and modification of LTY, LTL and ZSM-5 zeolites via the direct hydrothermal synthesis method, without using any organic structure directing agent or seeding gel. The original and modified zeolites were characterized by x-ray diffraction, Fourier-transformed infrared spectroscopy, solid state nuclear magnetic resonance spectroscopy, scanning electron microscopy, Brunauer–Emmett–Teller surface area analysis, and energy dispersive x-ray spectroscopy.

Moreover, the prepared zeolites were applied as catalysts in pyrolysis experiments in a bench scale horizontal reactor with Saskatchewan boundary dam coal, and their influences on the solid, liquid and gaseous products of this reaction were investigated using gas chromatography (GC), gas chromatography–mass spectrometry (GCMS) and CHNS/O elemental analysis. Furthermore, the influence of the catalysts on the pyrolysis kinetics was studied using thermogravimetric analysis.

**Acknowledgements**

I wish to express my sincere thanks and deep gratitude to my supervisor, Dr. Nader Mahinpey, for his invaluable guidance, helpfulness, inspiration and assistance throughout this M.Sc. project. I am also deeply indebted to him for understanding and supporting me at demanding situations.

I would like to thank Dr. Michael Schoel in the Faculty of Medicine, Robert Marr in the Department of Geology, Wade White and Johnson Li in the Department of Chemistry, all at the University of Calgary, for helping me with the SEM, EDX, XRD, NMR, GC-MS and FTIR tests required in this study.

I am also grateful to my committee members Dr. Joule Bergerson, Dr. Alex de Visscher and Dr. Abdulmajeed Mohamad for accepting to be in my defence committee and for their valuable suggestions.

I would like to thank the EERG group members, with whom I had the pleasure of working.

I gratefully acknowledge the financial support received from the Natural Sciences and Engineering Research Council of Canada (NSERC), Petroleum Technology Research Centre (PTRC) and the Department of Chemical and Petroleum Engineering at the University of Calgary.

Dedicated to my parents, my brother, and my wife

## Table of Contents

## List of Tables

## List of Figures

## List of Symbols, Abbreviations and Nomenclature

**Nomenclature**

| | |
|---|---|
| BJH | Barrett–Joyner–Halenda |
| BET | Brunauer–Emmett–Teller |
| EDX | Energy dispersive x-ray spectroscopy |
| FTIR | Fourier-transformed infrared |
| GC | Gas chromatography |
| GCMS | Gas chromatography–mass spectrometry |
| NMR | Nuclear magnetic resonance |
| LTL | Linde Type L |
| LTY | Linde Type Y |
| SEM | Scanning electron microscopy |
| SAR | Silicon to Aluminum ratio |
| SDA | Structure directiing agent |
| TGA | Thermogravimetric analysis |
| XRD | X-ray diffraction |
| ZSM-5 | Zeolite Secony Mobil-5 |
| A | Preexponential factor |
| $E_a$ | Energy of activation |
| k | Rate constant |
| n | Order of reaction |
| r | Rate of reaction |
| R | Universal gas constant |
| t | time |
| T | Temperature |
| x | Conversion |

# Chapter One: **Introduction**

## 1.1 Zeolites

Zeolites are a group of crystalline, hydrated aluminosilicates with well-defined micropores and regular structures. Zeolite was first discovered as a new type of mineral in 1756 by Axel F. Cronstedt (1722–1765), a famous Swedish mineralogist [1]. The unique properties of natural zeolites, such as their reversible water-adsorption capability, were gradually recognized through several years of practical application [2].

Efforts to synthesize silicates in the laboratory under hydrothermal conditions were initiated by Schafhautle in 1845, who reported synthesis of quartz when heating a silicate gel with water in an autoclave for the first time. From the years 1845 to 1937 many researchers investigated the hydrothermal conversion and synthesis of silicates. However, it was not until 1948 that Barrer successfully synthesized the first synthetic zeolite, with no natural counterpart, using the hydrothermal approach [3].

Although industrial synthetic zeolites were first reported by Union Carbide in 1954, the use of these materials in industry did not become important until the 1960s, when zeolite Y was developed and applied in the Fluid Catalytic Cracking (FCC) continuous process, where heavy hydrocarbon molecules break down to lighter molecules for gasoline production [4-5].

Synthesis of new zeolites and development of new techniques, as well as deep insight into zeolite properties such as thermal stability, acidity, hydrophobicity/hydrophilicity of surfaces, and ion-exchange capacity, has led to wide application of zeolites in industry.

Each zeolite is made up of a unique network of well-defined pores and channels which determine its physical and chemical properties. Having micropores of molecular size has given them adsorption, catalytic, and ion-exchange properties of great importance in several chemical industries, as well as in many other areas such as agriculture, animal food, and medicine [4,6]

[7]. Therefore, much research is aimed at the synthesis and modification of zeolites. The most recent Atlas of Zeolite Framework Types lists about 176 framework structures [8].

### 1.2 Coal Pyrolysis

Coal pyrolysis is the decomposition of coal through heating in the absence of oxygen to yield gases, liquids, and a solid residue (char or coke). This process is one of the significant approaches for the comprehensive utilization of coal. Due to the energy crisis, study of this process has been drawing more attention in recent years, and interest in making use of and upgrading of the products has grown.

Catalysis can be employed as a method of controlling coal pyrolysis and to improve the production of a number of desired chemicals, including aromatic compounds, through cracking of the volatile matter. Consequently, the synthesis and modification of new catalysts is of great significance [9-12].

Due to their unique properties, zeolites are vastly utilized in many processes in their original and modified forms [13-14]. For instance, zeolite Y (categorized under the faujasite family) is one of the most widely used zeolites in industrial processes such as fluid catalytic cracking, water treatment and pollutant removal [15]. Furthermore, involvement of zeolites with different characteristics and structures influences the yield and distribution of the catalytic coal pyrolysis products [16].

In this study, new approaches were adopted towards the template-free synthesis and modification of LTY, LTL and ZSM-5 zeolites via direct hydrothermal synthesis method, without using any structure directing agents (SDA) or seeding gel. The synthesized zeolites were characterized and employed as catalysts in the catalytic pyrolysis of Saskatchewan boundary dam coal. This type of coal is minable and can be found in southern parts of Saskatchewan. The

influence of the catalysts on the pyrolysis kinetics and products was studied using thermogravimetic analysis (TGA), bench scale reactor experiments, gas chromatography (GC), gas chromatography–mass spectrometry (GCMS) and CHNS/O elemental analysis.

### 1.3 Objectives

The main objectives accomplished in this research are enumerated below.

1. Direct hydrothermal synthesis of LTY zeolite using sodium silicate as silicon source in the absence of organic templates.
2. Direct hydrothermal synthesis of LTY, ZSM-5 and LTL zeolites using colloidal silica, a conventional silicon source, in the absence of organic templates.
3. Modification of the zeolites.
4. Investigation of the physical properties and characterization of the original and modified zeolites.
5. Investigation of the products of catalytic pyrolysis of Saskatchewan boundary dam coal using the prepared catalysts.
6. Investigation of the kinetics of the pyrolysis using thermogravimetric data.

# Chapter Two: **Literature Review**

## 2.1 Zeolites

Zeolites are a group of hydrated aluminosilicates with outstanding structural properties [17]. Their structure consists of a network of interconnected $SiO_4$ and $AlO_4$ tetrahedra linked to each other by sharing oxygen atoms. This network contains pores in the micropore range, with channels that extend in one, two or three dimensions. These channels and pores are occupied by water molecules, and cations (mainly alkali or alkaline earth metal ions). A pure silica ($SiO_2$) framework is neutral. The tetravalent Si can be replaced by trivalent Al to produce an aluminosilicate. Therefore, a negative charge is introduced into the framework for each substitution, and a cation is needed to counterbalance this negative charge. The presence of these cations, known as extra-framework cations, counterbalances the negative charge of the framework due to the presence of alumina, and it results in a strong electrostatic field on the internal surface of zeolites [18].

Zeolites can generally be expressed by the following formula:

$$M_{x/n}[(AlO_2)_x(SiO_2)_y].wH_2O \quad (1)$$

Where M represents the extra-framework cation of valance n, w is the number of water molecules and x and y are integers such that $y/x \geq 1$. The expression enclosed in the square brackets shows the anionic framework composition.

The very regular structure and pore sizes give these materials a sponge-like appearance (Figure 2.1). Zeolites differ in pore diameter, pore shape and the way they are interconnected. The pore size plays an important role in the application of the zeolites. Different pore sizes allow or prohibit the entrance of specific molecules to the system.

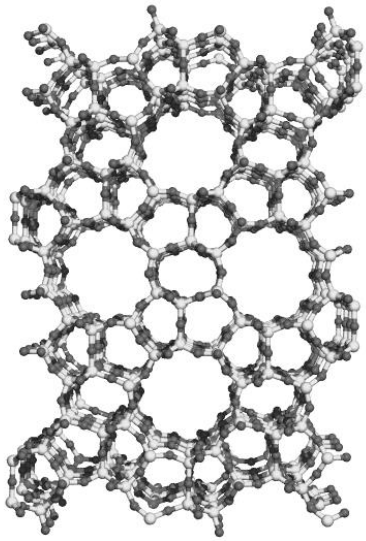

**Figure 2.1** Structure of Zeolite silicalite showing its pores [19]

Natural zeolites are the product of the chemical reaction between volcanic glass and saline water. This natural reaction is favored in temperatures between 27 °C and 55 °C, and pH values that typically range from 9 to 10. The completion of this reaction requires 50 to 50000 years [20]. Natural zeolites are rarely phase-pure and are contaminated by other minerals such as quartz, other zeolites, amorphous glass, etc. to varying degrees. Therefore, naturally occurring zeolites are not used in many important commercial applications, where uniformity and purity are essential.

On the other hand, synthetic zeolites, which are typically synthesized by nucleation from supersaturated starting gel compositions, are usually uniform and pure [20]. Preparation of the synthesis gel is the most important step of the synthesis of zeolites. A variation in the gel composition or synthesis process parameters can change the product or its properties. Therefore, the main factors affecting zeolite synthesis are: composition and homogeneity of the synthesis gel mixture, the nature of the reactants, crystallization and aging temperatures and their durations, the template molecule, and the pH of the system.

Currently, natural zeolites are widely used in the fields of drying, separation of gases and liquids, softening of hard water, and treatment of sewage [15].

Typically, water molecules occupy the internal voids of the zeolite. The fact that zeolites retain their structural integrity upon loss of water makes them different from other porous hydrates, such as $CaSO_4$.

The crystalline nature of the zeolite framework ensures pore size uniformity throughout the crystal and can discriminate against molecules with dimensional differences less than 1 Å, giving rise to the name molecular sieves [21].

Impregnation of zeolites with metallic cations including transition metals such as Co, Ni, Mn, Ag, etc. can give rise to new properties. Preparation of the impregnated zeolites has led to the development of several new applications [22-23].

Since natural zeolites cannot meet the huge demand in industry, it is inevitable that synthesized zeolites are utilized as well as natural zeolites. The most recent Atlas of Zeolite Framework Types lists about 176 framework structures [8].

**2.2 History**

Zeolite was first discovered as a new type of mineral in 1756 by the Swedish mineralogist Cronstedt, who observed the vapor release upon heating of a stone nowadays called stilbite. The word “zeolite” is derived from two words “zeo” and “lithos” which are Greek words for “boil” and “stone” because, when gently heated, natural zeolite stones lose water rapidly and thus seem to boil [24]. After several years of practical applications, the main properties of natural zeolites such as their reversible water-adsorption capability were recognized [2].

During utilization of ion-exchange capacity of some soils at the end of the $19^{th}$ century, it was found that natural zeolites exhibited similar properties, and some cations in natural zeolites could be ion-exchanged by other cations. Moreover, it was observed that natural chabazite could

adsorb water, methanol, ethanol, and formic acid vapor, but it could not readily adsorb acetone, diethyl ether, or benzene. The importance of these features was soon recognized and natural zeolites found applications as adsorbents and desiccants. Later, natural zeolites were also used widely in separation and purification of air [24].

Efforts to synthesize silicates in the laboratory under hydrothermal conditions were initiated by Schafhautle in 1845, who reported the synthesis of quartz by heating a silicate gel with water in an autoclave for the first time. Levynite (LEV) was the first synthetic zeolite that was hydrothermally synthesized by St Claire Deville in 1862. Schulten reported the synthesis of analcime (ANA) in 1882. Several other zeolites were synthesized in succeeding years [18]. However, the early synthetic work was not very well recognized because essential data for identification was not available. The synthesis of zeolites was continued by the pioneering work of Barrer that began in the 1940s and initially investigated the conversion of known mineral phases in strong salt solutions at rather high temperatures (ca. 170–270°C). Later in 1948, Barrer synthesized the first synthetic zeolite with no natural counterpart using the same approach [25-26, 3].

In the late 1940s, Milton and co-workers successfully synthesized zeolites A (LTA), X (FAU), and P (GIS) through hydrothermal crystallization of reactive alkali metal aluminosilicate gels at low temperatures (ca. 100°C) and autogenous pressures under alkaline conditions with pH values higher than 12 [27-28]. By 1953, they were able to synthesize 20 zeolites, 14 of which did not have natural counterparts, and developed synthetic methodologies which initiated the zeolite technology [29].

Significant progress in the production of zeolites was made from 1954 to the early 1980s. Zeolites with low, medium, and high silica to alumina ratios (SAR) were widely explored, which

greatly facilitated the applications of zeolites and led to innovations in industrial processes. Synthesis of zeolite Y by Breck et al., which represented higher thermal stability and acidity, played a significant role in the catalysis of hydrocarbon conversion. Moreover, in 1967 Milton synthesized new type A, X and Y zeolites, which led to their commercial applications as selective adsorbents and catalysts [5]. From then on, many different zeolite structures with a variety of Si/Al ratios such as zeolite Y (Si/Al=1.5-3), L (Si/Al=3-6), ZSM-5 (Si/Al>12) have been synthesized.

The use of organic components, nowadays known as structure directing agents or templates, in the synthesis of zeolites played an essential role in initiating the significant advances of zeolite synthesis. For instance, high-silica zeolite ZSM-5 (MFI) was initially obtained using the tetrapropylammonium (TPA) cation [30].

Synthesis of new zeolites and development of new techniques, as well as deep insight into zeolite properties such as thermal stability, acidity, hydrophobicity/hydrophilicity of surfaces, and ion-exchange capacity, has led to wide application of zeolites in industry. These zeolites include those that are synthesized, such as zeolite A, zeolite X, zeolite Y, zeolite L, ZSM-5, and those that are natural, such as mordenite, chabazite, erionite and clinoptilolite. These materials have found broad application as commercial adsorbents for drying and purification of gases and for bulk separation processes such as the separation of normal-/iso-paraffins, isomers of xylenes and olefins, and $O_2$ from air. Zeolites have also been widely used as catalysts for petroleum refining and petrochemistry, and as ion exchangers [5].

**2.3 Structure**

The special properties of zeolites, such as their ion-exchange, sorption, shape selectivity, and catalytic properties are essentially determined by their structural characteristics such as pore

size, pore volume, ion-exchange capacity, channel system, etc. [31]. Consequently, structural analysis is a fundamental step in exploiting zeolites.

Characteristics of the framework type alone can explain many of the observed properties of a zeolite. The framework type describes the connectivity (topology) of the framework tetrahedra without reference to chemical composition, and defines the size and shape of the pore openings, as well the dimensionality of the channels, and the types of cation sites available. However, the chemical composition of the framework, the nature of the species within the channels, and the type of post-synthesis modifications applied are important factors in determining the specific properties of a particular zeolite. For example, a large cation can block or reduce the effective size of a pore opening, a small cation might distort a pore opening, and a sorbed species can influence the catalytic, magnetic, or electronic properties of a zeolite [13].

Precise understanding of the structure, the nature of the distortion of a framework from ideal symmetry and the location and distribution of the extra-framework species are fundamental to the understanding of zeolite chemistry. Such understanding can be obtained to some extent through surface area and sorption analysis (pore size), electron microscopy (symmetry, faulting), and powder diffraction or other similar characterization techniques.

In 1970 Meier and Olson proposed a classification for zeolites which has gained wide acceptance and is used as a reference in zeolite studies [8]. In this system a three-letter code (e.g., FAU) is assigned to characterized framework types by the Structure Commission of the International Zeolite Association according to the IUPAC standards on zeolite nomenclature [32, 33]. A framework type simply gives information on the connectivity of the constituting tetrahedra of the framework in the highest possible symmetry. However, framework type does not describe the composition and observed symmetry in the zeolite.

The codes are typically derived from the name of the zeolites. For example, FAU from the mineral faujasite, LTL from Linde Type L, and ZSM-5 from Zeolite Socony Mobil Five. Information pertinent to the reference zeolite framework types is published in the Atlas of Zeolite Framework Types [8].

**2.4 Characteristics of zeolite framework types**

The feature that is common to zeolite or zeolite-like materials is that they all have three-dimensional framework structures which consist of $TO_4$ tetrahedra (where T is silicon or aluminum) interconnected with oxygen atoms. This framework structure is relatively open and characterized by the presence of channels and cavities. A description of a zeolite structure most often begins with a description of the framework type that gives information about the size of the pore openings and the dimensionality of the channel system. Pore openings are characterized by the size of the ring that defines the pore. The pore opening is designated an n-ring, where n is the number of T-atoms in the ring. An 8-ring is considered a small pore opening, a 10-ring a medium opening, and a 12-ring a large opening.

Zeolite frameworks usually consist of a number of common structural features (cages, channels, chains, and sheets) with different connectivity which distinguishes different zeolite structures. These features are introduced with designations such as α-cavity and β-cage, and pentasil unit and have crept into common usage and may be found in different zeolites. Some of these subunits are shown in Figure 2.2. In these drawings, oxygen atoms have been omitted for clarity.

These units are sometimes described by designations based on the n-rings defining their faces. Some of these designations are also presented in Figure 2.2. For example, a truncated octahedron (sodalite cage), whose surface is defined by six 4-rings and eight 6-rings, would be named a $[4^6 6^8]$ cage.

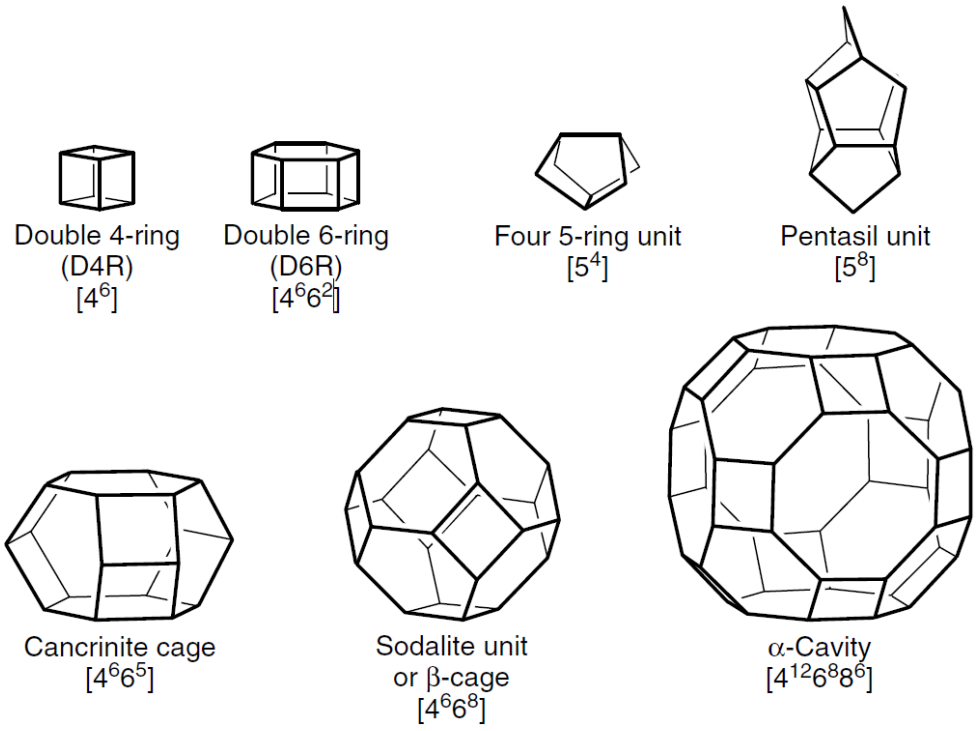


**Figure 2.2** Some subunits and cages or cavities that recur in several framework types

In this research, three zeolite types, LTY, LTL and ZSM-5 were synthesized, modified, and characterized. Following in this chapter, a brief summary on the structure of these zeolites is given. The modification techniques applied and the influence of the use of these materials as catalysts in coal pyrolysis reaction are explained later in Chapter 4.

### *2.4.1 Linde Type Y (LTY) zeolites*

This zeolite framework (Figure 2.3) consists of sodalite cages arranged in a similar way to the carbon atoms in diamond, and they are linked to one another by double 6-rings. This creates a configuration known as the supercage, with four tetrahedrally oriented, 12-ring pore openings and a 3-dimensional channel system. There is a center of inversion in each of the double 6-rings, so the layers of sodalite cages are related to one another by inversion and form a symmetric network. Zeolite Y structure has a large void volume and 12-ring pore openings

forming a 3-dimensional channel system. Moreover, the FAU framework type is thermally stable and ideal for many catalytic applications [8].

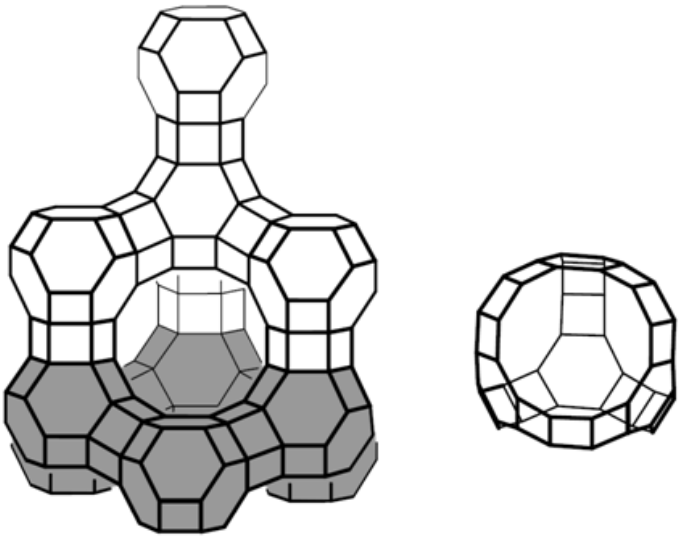

**Figure 2.3** The FAU framework type and its supercage [8]

### *2.4.2 Zeolite Socony Mobil–5 (ZSM-5) zeolites*

The framework type of the zeolite ZSM-5 (Figure 2.4) consists of [$5^8$] units that are linked to form pentasil chains. Connections of mirror images of these chains are by oxygen bridges and will then form corrugated sheets with 10-ring holes (e.g., the gray sheet perpendicular to x in Figure 2.4). Each sheet is linked by oxygen bridges to the next sheet to form the 3-dimensional structure. The connection of these sheets produces a 3-dimensional 10-ring channel system within the zeolite framework. The 10-ring, rather than 12-ring, pore openings is one of the reasons the shape selectivity for sorption and catalysis behaviors are distinctly different from that of FAU and LTL type zeolites [8]. ZSM-5 has found many applications in refinery and petrochemical processes [34].

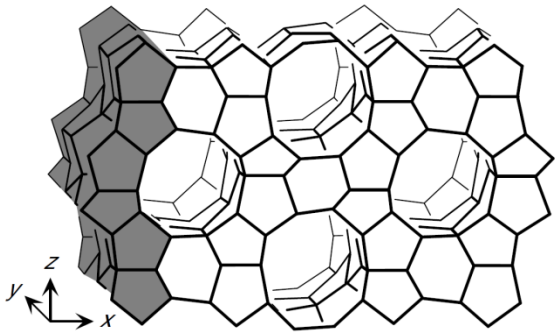


**Figure 2.4** The MFI framework type with pentasil chains [8]

### *2.4.3 Linde Type L (LTL)*

The LTL framework is based upon the alternatively connected cancrinite cages and double 6-rings (D6R) forming the -can-D6R-can- columns. Connection of six columns of this type along the z axis gives rise to a 3-dimensional framework that has 12-ring pore openings and an aperture of approximately 7.1*7.1 Å (figure 2.5) [35-37].

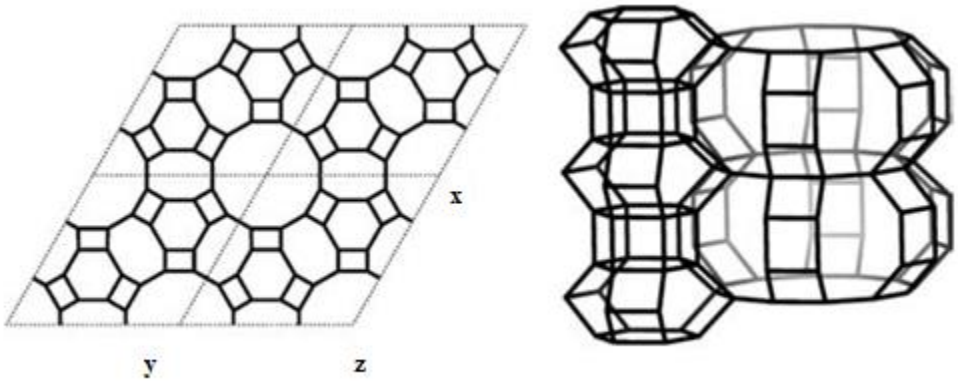


**Figure 2.5** LTL framework and the -Can-D6R-Can- Column [8]

## 2.5 Synthesis of zeolites

Zeolites have found vast applications in many commercial and industrial processes. Therefore, synthesis of zeolites has become an important field of research because of the special

properties of zeolites, with uniform micropores in catalysis, adsorption and separation. Moreover, zeolites are finding new applications in electronics, chemical sensors, medicine, etc. [38-40].

### *2.5.1 Hydrothermal synthesis of zeolites*

After the pioneering work of Barrer and Milton, which led to successful hydrothermal synthesis of zeolites, this technique has become the basic route for the synthesis of zeolites. Hydrothermal synthesis typically refers to reactions taking place at high temperatures and elevated pressures (>100°C, >1 bar) in aqueous solutions in a closed system. However, the hydrothermal synthesis covers all temperatures and pressures above room temperature and 1 bar [41-42].

The hydrothermal method is most commonly employed to synthesize zeolites. Zeolite Y, L and ZSM-5 can be synthesized through the hydrothermal process via equation (1) [2].

$$SiO_2 + Al_2O_3 + Na_2O + H_2O \rightarrow \text{Aluminosilicate gel} \rightarrow \text{Crystalline zeolites} \quad (1)$$

The resultant zeolite obtained by this method is in its $Na^+$ (sodium) form and, for specific purposes, may need to be modified and transformed into its other forms by various techniques, including ion-exchange and thermal treatment processes. Generally, ammonium ($NH_4^+$) form of the zeolite is used to obtain its acidic form. In addition, metallic ions such as silver, nickel or platinum can be deposited via impregnation [22].

Considering its applications at elevated temperatures (e.g. catalytic fluid cracking), high hydrothermal stability and acidity are preferred for zeolite Y, which can be improved by post-secondary treatments such as dealumination or ultra-stabilization. For the dealumination process, the $NH_4^+$ form of zeolite is heated in a steam-containing atmosphere, resulting in deammoniation and generation of Bronsted acidic bridging protons in the framework [43]. In the meantime, aluminum is removed from the framework and enters the pores. Vacant tetrahedral sites appear,

and silicon atoms migrate to fill these void sites. Consequently, a more hydrothermally stable framework with an increased SAR is formed [44].

The advantages associated with hydrothermal synthesis have resulted in an increasing interest in utilization of this method. The hydrothermal synthesis is classified into two types: subcritical and supercritical, according to the reaction temperature. In subcritical synthesis, temperature varies between 100 to 240°C, while in supercritical synthesis, temperature could be as high as 1000 °C and pressure may be elevated up to 3000 bar. In supercritical conditions, the thermodynamic behavior and transport properties of supercritical water deviate significantly from those of ambient water [45]. In this research zeolites were synthesized under subcritical hydrothermal conditions.

### *2.5.2 Hydrothermal apparatus*

The hydrothermal synthesis of zeolite materials is generally performed in sealed vessels. The high autogenous vapor pressure buildup in these vessels at high temperatures (>100°C) is a major safety concern associated with this method. In this research, a Teflon-lined acid digestive autoclave (produced by Parr Instrument Company), and Teflon bottles were used for the synthesis of LTL, ZSM-5 and LTY zeolites. Moreover, stainless steel (316 SS) was used to fabricate a new autoclave for the preparation of the dealumined type Y zeolites.

### *2.5.3 Important factors affecting the synthesis*

While the hydrothermal synthesis of zeolites follows a straightforward procedure, the synthetic chemistry of zeolites is very complicated. Most zeolites are formed as metastable phases under hydrothermal conditions. Crystallization of zeolites is known as one of the most complex chemical problems in crystal nucleation and growth [2]. The zeolite crystallization involves complex reactions, such as nucleation and crystallization. Several variables affect the formation of a specific zeolite phase, such as starting gel composition, reactant sources, Si/Al

ratio, alkalinity, water content, inorganic cations, structure directing agents or templates, solvents, temperature and duration of aging and crystallization, stirring, and seeding [31]. This section will present a summarized discussion of some of the mentioned synthetic parameters.

2.5.3.1 Batch composition

In recent years, several research investigations have been aimed at studying the various parameters that influence the synthesis pathway and the characteristics of the end product [46-47]. The results of these studies emphasized that the chemical composition of the reaction mixture was one the most influential parameters in controlling the particular properties of the zeolite [48-50].

Breck's work showed how the batch composition significantly affected the formation of zeolites with a particular structure type [18]. Berger et al. showed that the silicon (Si) / aluminum (Al) ratio (SAR) of zeolite Y increased with increases in the silica ($SiO_2$) / alumina ($Al_2O_3$) ratio in the starting gel composition. Nevertheless, their research showed that further increases in the molar ratios of $SiO_2/Al_2O_3$ beyond five did not result in further increases in the SAR of the produced type Y zeolite [51].

2.5.3.2 Silicon and Aluminum sources

The chemical and physical characteristics of the reactants have a significant effect on the crystallization of zeolites. Different chemicals used as silicon sources in the synthesis of zeolites differ in reactivity and solubility. The influence of reactant sources is well documented in the early synthetic work [8]. The silicon sources commonly used in the synthesis of zeolites are sodium water glass, colloidal silica, fumed silica, tetramethylorthosilicate (TMOS), and tetraethylorthosilicate (TEOS). Different crystallization rates, crystal sizes and particle size distributions occur in the synthesis of zeolites when different silica sources are used [52].

For instance, it was found that different surface areas of the silicon source could affect the synthesis of the zeolites by influencing parameters such as crystallization rate, the crystal size, and the particle size distribution as in the synthesis of zeolite A (LTA) [2].

Aluminum sources also influence the zeolite crystallization. The aluminum sources commonly used in zeolite synthesis are sodium aluminate, aluminum hydroxide, aluminum isopropoxide, aluminum nitrate, and aluminum sulfate. Sano and co-workers investigated the influence of different aluminum sources on the hydrothermal synthesis of high-silica mordenite in the presence of tetraethylammonium and fluoride ions at 170 °C. It was found that pure MOR-type zeolite could be obtained when $AlCl_3$ and $Al_2NO_3$ were used as an Al source, whereas zeolite beta (BEA) was prepared as the main product or a byproduct with $Al_2(SO_4)_3$ [53].

2.5.3.3 Si/Al ratio

The Si/Al ratio in the starting gel composition is an important parameter in determining the structure and composition of the crystallized product. In general, zeolites with low Si/Al ratio (Si/Al $\leq$ 5), for example zeolites A (LTA) and X (FAU), are prepared from gel compositions with low Si/Al ratio and strong alkalinity, while high-silica zeolites (Si/Al>5) such as ZSM-5, are obtained from gel compositions with high Si/Al ratio and weak alkalinity. However, due to the complexity of the zeolite synthesis reactions, there is no quantitative correlation of the Si/Al ratio in the initial reaction system and that in the final product. Therefore, it is not possible to adjust the Si/Al ratio in the zeolite product by varying the Si/Al ratio in the initial reaction mixture [13]. Well-optimized conditions, or in some instances use of specific structure-directing agents (SDA), are typically required to obtain the desired Si/Al ratio in the product [21].

2.5.3.4 Alkalinity

Most zeolites are crystallized from basic $Na_2O$-$Al_2O_3$-$SiO_2$-$H_2O$ mixtures. In the zeolite synthesis systems, the alkalinity is defined as $OH^-$/Si ratio. Higher alkalinity increases the

solubility of the Si and Al sources, decreases the polymerization degree of the silicate anions, and accelerates the polymerization of the polysilicate and aluminate anions. Consequently, at higher alkalinities, induction and nucleation periods will shorten and the crystallization of zeolites accelerates [13].

2.5.3.5 Water content

Water acts as a solvent in the hydrothermal synthesis of zeolites. Generally, for hydrothermal synthesis of a particular zeolite, the amount of water varies within a specific range. However, the changes in concentration of reactants due to the variations of the water content affect the crystallization of the zeolites. Early work of Breck showed that the water content can change the final product [18]. Generally, overall dilution of the primary synthetic gel leads to lower supersaturation, which is favorable for crystal growth. Subsequently, large crystals can be obtained.

2.5.3.6 Organic templates

Structure directing agents (SDAs), such as tetrametylammonium hydroxide (TMAOH), and tetrapropylammonium hydroxide (TPAOH), are sometimes necessary for the synthesis of pure forms of a number of zeolites. SDAs have also been used to synthesize zeolites with higher SARs or controlled particle sizes [54-55].

Organic molecules act by organizing the oxide tetrahedra into a particular geometry around themselves and thus provide initial building blocks for a particular structure. Lok et al. studied the role of the organic templates in the synthesis of zeolites [56]. Their research suggested that both gel chemistry and template species play significant roles in the formation of a specific structure. They also suggested that templating is effective only in the right gel chemistry conditions. Use of templates for obtaining zeolites with specific properties has also

been reported. Ferechiche and Warzywoda synthesized zeolite Y with particle sizes as large as 120μm with TMAOH as the organic SDA [57].

Removal of SDAs from the structure of zeolites is challenging, as the structure of zeolite may become partially damaged or collapse. Moreover, due to the high price of SDAs, their use is only limited to special purposes, and template-free synthesis of zeolites is usually preferred.

2.5.3.7 Aging

Aging is referred to as the period from homogeneous mixing and preparation of the starting gel to the onset of heating to the crystallization temperature. Several studies revealed that aging affects the gel chemistry and, consequently, the nucleation and crystal growth kinetics of zeolites [58]. Even though aging processes are not yet well understood, it appears that aging has significant impacts on the nucleation and crystallization of zeolites. These impacts include increasing the nucleation rate, reducing duration of crystallization, reducing the crystal size, and improving the crystal population [13]. Okubo et al. studied the effect of aging on the formation of aluminosilicate species in the hydrogel prior to crystallization of a FAU type zeolite. Results of their study showed that shorter aging periods resulted in the formation of other phases, including sodalite (SOD), chabazite (CHA), and analcime (ANA) [59]. In this study, it was observed that the formation of pure FAU type zeolite phase required at least 1 day of aging.

2.5.3.8 Crystallization temperature and time

Temperature is another important parameter in the synthesis of zeolites. Significant attention has been paid to the crystallization temperature due to its strong effect on the formation of zeolites. A particular zeolite phase typically can only be obtained within a specific temperature range. Both nucleation and crystal growth are strongly influenced by the crystallization temperature [60-61]. The nucleation and crystal growth rates both increase at

higher temperatures. However, crystal growth rate increase is more significant than the nucleation rate, which leads to higher growth rates and larger crystals can be obtained [62-63].

Crystallization time is another important parameter in the hydrothermal synthesis of zeolites. In general, crystallinity increases with time. However, it is important to note that zeolites are thermodynamically metastable phases, and prolonged crystallization times may change the synthesis product. For instance, prolonged crystallization time causes the zeolite A (LTA) and zeolite X (FAU) to be replaced by other phase zeolites sodalite (SOD) and P (GIS), respectively [21].

2.5.3.9 Stirring

In the laboratory, zeolites are more commonly synthesized under static conditions. However, several studies have shown that stirring can impact the crystallization kinetics, in particular the crystal size. Smaller crystals can be synthesized by stirring since supersaturation can be faster achieved due to the accelerated mass transfer. Furthermore, it is observed that stirring modifies the selectivity of the different zeolite phase formations. For instance, formation of zeolite A (LTA) is preferred over zeolite X (FAU) in a stirred system, and ZSM-5 is favored instead of ZSM-22 from an unstirred synthetic system [64].

2.5.3.10 Applications of zeolites

Zeolites are extensively used as ion exchangers in laundry detergents to remove calcium and magnesium from water by exchanging them for sodium ions present in the zeolite. Moreover, zeolites are utilized as adsorbents in the purification of gas streams for removal of water and volatile organic species, and in the separation of different isomers and gas mixtures. These materials have also found applications in catalysis of several chemical reactions, as well as in medicine [65-66]. However, in this thesis, we aimed to investigate the catalytic effect of the prepared LTY, ZSM-5 and LTL type zeolites in coal pyrolysis.

## 2.6 The role of a catalyst

A catalyst is referred to as a material which changes the rate of a reaction without itself being consumed. Catalysis is an exceptional phenomenon in the sense that additions of very small portions of catalyst in the reaction can convert hundreds of times the catalyst weight of chemicals. Moreover, catalysts can direct a chemical reaction to increase the amount or the production rate of a specific product; in other words, to accelerate a chemical reaction or to provide selectivity.

Special characteristics of the zeolites, such as their ability to adsorb and transform molecules in their inner voids, have given them distinguishable properties with regard to activity and selectivity in the catalyst industry [67]. An important class of reactions assisted by zeolites is the acid-catalyzed reactions. Zeolites exhibit Bronsted acidic sites and are also sometimes referred to as solid acids. Moreover, zeolite frameworks can host oxides of transition metals and accommodate oxidation and/or reduction reactions. The chemical composition, structure, size and particular pore system of a zeolite determines its catalytic properties. Moreover, different zeolites adsorb different molecules and produce different products, and are consequently said to induce shape selectivity, which makes it possible to direct and influence the hydrocarbon transformation reactions in a way other than that which occurs in the absence of catalysts [68].

Application of synthetic zeolites X and Y in the cracking of heavy crude oil into lighter valuable products resulted in a major increase in the yield of gasoline and was a breakthrough in the catalysis and petrochemical industry [69]. Currently, synthetic zeolites are utilized in industry as catalysts for numerous reactions, especially in the field of oil refining and basic petrochemistry.

## 2.7 Coal Pyrolysis

Coal pyrolysis is the decomposition of coal through heating in the absence of oxygen to yield gases, liquids, and a solid residue (char or coke). This process is one of the significant approaches for the comprehensive utilization of coal. Due to the energy crisis, study of this process has been drawing more attention during recent years, and interest for making use of and upgrading of the products has grown.

Pyrolysis as the initial step in several coal utilization processes such as combustion, gasification, liquefaction, and carbonization greatly influences the later steps of these processes. Coal pyrolysis products are highly affected by the operating conditions and by the nature and properties of the coal [70].

During pyrolysis, coal undergoes different chemical and physical changes which are influenced by several parameters such as rank, composition, particle size, heating rate, temperature, and the atmosphere in which pyrolysis occurs. Coals of different ages have different chemical compositions, which results in different structures. The differences are even evident within a certain rank or age group of coals, such as lignites or bituminous coals, where the structure varies depending on the geographical conditions in which a particular coal was formed [71]. Furthermore, the influence of particle size, temperature, pressure and heating rate on the pyrolysis reaction has been reported [72-75].

Generally, two processes occur when coal is heated. One is depolymerziation, which leads to the formation of water vapor, gas and tars, and the other is condensation, or repolymerization, through which char or coke is produced [76].

During the pyrolysis process, rupture of the bonds that attach the functional groups to aromatic and hydroaromatic units of the coal structure results in the formation of gases such as CO, $CO_2$, $H_2O$, $CH_4$, $C_2H_4$, etc. Furthermore, free radicals are released as the crosslinks within the structure of the coal break. Presence of these radicals and the reactions they involve greatly affect the distribution and overall yield of the products [77-78].

The liquid product, also known as coal pyrolysis oil, has the potential to be used as a feedstock for petroleum refinery units in the manufacture of valuable chemicals and gasoline [79-80].

Catalysis can be employed as a method of controlling coal pyrolysis and to improve the production of a number of desired chemicals, including aromatic and alkylhydrocarbons (phenols) through cracking of the volatile matter. Consequently, the synthesis and modification of new catalysts is of great significance [9-12]. Moreover, future upgrade of the pyrolysis oil to hydrocarbon fuels may become possible. Catalysts may also increase the potential uses of the gaseous product of the pyrolysis by changing the nature and distribution of the produced gasses.

Due to their unique properties, zeolites are vastly utilized in many processes in their original and modified forms [13-14]. For instance, zeolite Y (categorized under the faujasite family) is one of the most widely used zeolites in industrial processes such as fluid catalytic cracking, carbon dioxide capture, water treatment and pollutant removal [15]. Furthermore, involvement of zeolites with different characteristics and structures influences the yield and distribution of the catalytic coal pyrolysis products [16].

Study of coal pyrolysis kinetics is essential for the understanding of the mechanism and modeling of the pyrolysis process. Isothermal and non-isothermal thermogravimetric (TG) analyses are broadly carried out to investigate the kinetics of coal pyrolysis reactions.

The TG technique is based on the mass differentials during the pyrolysis experiment as a function of temperature in non-isothermal pyrolysis and as a function of time in isothermal pyrolysis.

Several studies have investigated coal pyrolysis kinetics. However, there are very few data available on the detailed analysis of catalytic coal pyrolysis. Fitting method is usually used to obtain information on the reaction mechanism. Apparent energy of activation ($E_a$) and its dependent parameters can be obtained by this method [81-82]. Other techniques, such as the mathematical methods developed by Coats-Redfern, MacCallum-Tanner, and van Krevelen are commonly used to estimate the kinetics parameters of pyrolysis reactions [83]. In this study, a reaction mechanism fitting method using the integrated core model and a single heating-rate analytical model by Coats-Redfern were used to investigate the kinetics of the isothermal and non-isothermal stages of the pyrolysis reaction, respectively.

# Chapter Three: **Materials and Experimental Procedures**

## 3.1 Materials

The following materials were used: silica sol (40% w/w $SiO_2$, Ludox HS40, Sigma-Aldrich, St. Louis, MO); sodium silicate solution (10.6 % w/w $Na_2O$, 26.5 % w/w $SiO_2$, 62.9 % w/w $H_2O$, Sigma-Aldrich, St. Louis, MO); sodium aluminate (38.8% w/w $Na_2O$, 54.2% w/w $Al_2O_3$, 8% w/w $H_2O$, Strem Chemicals, Newburyport, MA); potassium hydroxide (reagent grade, 90% KOH, Sigma-Aldrich, St. Louis, MO); sodium hydroxide (> 99% w/w NaOH, Alphchem, Mississauga, ON); aluminum hydroxide (reagent grade, Sigma-Aldrich, St. Louis, MO); calcium chloride dihydrate (> 99%, BDH, VWR, Canada); nickel(II) nitrate hexahydrate (> 97%, Sigma-Aldrich, St. Louis, MO); and, distilled water. Moreover, Saskatchewan boundary dam (BD) coal was used in the pyrolysis experiments.

## 3.2 Synthesis of zeolites

### *3.2.1 Synthesis of zeolite LTY using sodium silicate*

A direct hydrothermal synthesis method with a new starting gel composition was used to produce pure zeolite Y. The starting gel composition of $5.35Na_2O{:}1Al_2O_3{:}3.93SiO_2{:}154H_2O$ provided the pure product and was used throughout this study.

In a typical procedure, 2.43 g of sodium aluminate and 2.57 g of sodium hydroxide were dissolved in 26.55 ml of distilled water. The resultant solution was heated to its boiling point under agitation for 0.5 h, until a clear solution was obtained. After cooling down to room temperature, 6.25 ml of the sodium silicate solution (10.6 % w/w $Na_2O$, 26.5 % w/w $SiO_2$, 62.9 % w/w $H_2O$) was added dropwise to the solution and the solution was aged at room temperature for 24 h, and subsequently, the mixture was transferred into a Teflon bottle and then kept at 100°C for 48 h. After the autoclave cooled down, the solid product was filtered and washed with distilled water repeatedly to remove the unreacted chemicals. After drying at 100°C for 3 h,

zeolite Y powder was obtained.

### *3.2.2 Synthesis of zeolite LTY using colloidal silica*

The gel composition of $4Na_2O:1Al_2O_3:6SiO_2:180H_2O$ was used for the template-free synthesis of zeolite Y, using silica solution as the silicon source [84]. To prepare the desired starting gel composition, 2.08 g sodium aluminate and 2.32 g sodium hydroxide were added to 25 cc of water. The solution was stirred and heated to its boiling point until a clear solution was obtained. The mixture was cooled down to room temperature and water was added to make up for the water lost through evaporation. Subsequently, 9.72 g of silica solution was added drop-wise to the solution under vigorous agitation. After mixing for half an hour, the mixture was transferred into a Teflon bottle and aged for 24 hours without stirring. The bottle was then heated to 100°C in an oven for 48 hours without stirring. After the thermal stage the solution was cooled down to room temperature and the solid product was filtered by vacuum. The solution was washed with distilled water to remove unreacted chemicals and then dried at 100 °C for 3 hours.

### *3.2.3 Synthesis of zeolite ZSM-5*

This zeolite is typically synthesized with the aid of Tetrapropylammoniumbromide (TPABr), which is an organic structure directing agent or organic template [85-86]. The templates are generally unrecoverable, corrosive, expensive and difficult to remove from the zeolite structure without causing structural defects [87].

In this study a molar gel composition of $7.15Na_2O:1Al_2O_3:47.61SiO_2:1190H_2O$ was found to produce ZSM-5 with high crystallinity and surface area. Preparation of this starting gel was carried out by a procedure similar to that of zeolite Y starting gels, using 0.43g sodium hydroxide, 0.18g sodium aluminate, 6.67cc silica solution and 16cc water. This solution was aged for three days in a Teflon bottle at room temperature and crystallized for four days in a Teflon-lined Parr digestive vessel at 180°C. Subsequently, zeolite powder was obtained after

filtration, washing, drying and calcination.

The original, ammonium and hydrogen forms of this zeolite are denoted by ZSM-5, $NH_4$ZSM-5 and HZSM-5, respectively.

### *3.2.4 Synthesis of zeolite LTL*

The starting gel composition of $10K_2O{:}60SiO_2{:}1Al_2O_3{:}400H_2O$ was used to synthesize zeolite L. To prepare this gel composition, 5.61g potassium hydroxide was dissolved in 25.83g hot water, and 0.78g aluminum hydroxide was subsequently added. The resulting mixture was heated under severe agitation until a clear solution was obtained. The mixture was cooled, and evaporated water was compensated for with the addition of fresh water. Afterwards, 15cc silica solution was added dropwise to the previous mixture under agitation to complete the starting gel composition. The starting gel composition was then transferred to an oven at 175°C in a Teflon-lined Parr digestive vessel and synthesized zeolite L particles were retrieved after 72hr, similar to zeolite Y particles. The original and hydrogen form of this zeolite are denoted by LTL and HLTL, respectively.

### *3.2.5 Preparation of the modified zeolites*

Different zeolites can be modified to become applicable for specific processes. In this thesis, three zeolite types Y, L, and ZSM-5 were prepared, modified and characterized to give a better understanding of the impacts of modifications on the zeolite powders. Later, these zeolites were used as catalysts in coal pyrolysis experiments, and their influence on the products and kinetics of the reactions were investigated.

#### 3.2.5.1 Ion Exchange

Extra framework cations in the zeolite structure are ionically bonded to the zeolite framework and can be displaced by other cations though ion exchange. To change the resultant

zeolites to their calcium ($Ca^{2+}$) and ammonium ($NH_4^+$) forms, the following ion-exchange procedures were applied.

3.2.5.1.1 Changing to $NH_4^+$ form

Five grams of the sodium forms of the synthesized zeolites were mixed with 40 ml of 1.5 M ammonium nitrate solution at 75°C for 1 h. The attained zeolite powders were filtered and washed twice with distilled water. The zeolite powders were then dried at 100°C for 2 h. This procedure was repeated two more times, using 40 ml portions of the 1.5 M ammonium nitrate solution.

3.2.5.1.2 Changing to $Ca^{2+}$ form

Five grams of the obtained sodium or ammonium form of the zeolites were mixed with 100 ml of 1.5 M calcium chloride at 75°C for 1 h. The particles were filtered, washed and dried at 100°C for 2 h. The exchange procedure was repeated twice more to ensure maximum ion exchange.

3.2.5.2 Changing to H and dealuminated form

The $NH_4$ form of zeolite Y is typically the starting material for obtaining hydrogen (H) and ultra-stable (USY) forms of this zeolite in a process that involves calcination and steaming at high temperatures. Ultra-stable is a term referred to zeolites that have been extensively dealuminated. Calcination at temperatures above 500°C may damage the zeolite structure. To avoid the collapse of the structure during calcination, a two-step method can be used [88]. However, due to higher thermal stabilities of zeolites L and ZSM-5, they can be modified to their H form by single step calcination.

The high-temperature calcination of $NH_4Y$ with water vapor is used to achieve dealumination and stabilization of the zeolite structure. Heating to 260°C decomposes the $NH_4^+$

species and hydrogen containing intermediate is formed. Due to the small size and strong polarizing ability of H+, this cation can bond with the framework oxygen and form hydroxyls.

In the case of zeolite Y, the H form was prepared by heating the $NH_4^+$ form of zeolite Y to 260°C for 4 h followed by calcination at 550°C for 2 h. Moreover, to obtain the dealuminated (H-USY) form of the zeolite from the $H^+$ form, a stainless steel batch reactor with a capacity of 280 $cm^3$ was designed, as shown in figure 3.1. One milliliter of distilled water was poured at the bottom of the reactor, and the zeolite powder was placed in the reactor on a tripod, preventing direct contact of zeolite with water. The reactor was then sealed and put in an oven at 260°C for 2 h. The temperature was further increased to 550°C for another 2 h and, after cooling down to room temperature, the sample was collected and dried at 100°C for 3 h.

Furthermore, the H form of zeolites L and ZSM-5 were prepared by the calcination of their $NH_4^+$ form at 600°C for 4 hours.

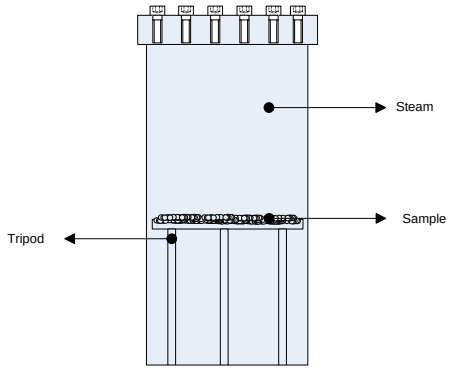


**Figure 3.1** Schematic of the batch reactor used for the preparation of dealuminated Y type zeolites

3.2.5.3 Impregnation of Nickel Oxide

Zeolites can be impregnated with nickel by exchanging out the parent sodium ions from the structure of the parent zeolite. In this study, a different method was used to achieve the

impregnation of nickel(II) oxide (NiO). Impregnated zeolites were synthesized by adding a nickel nitrate solution to the starting gel right before the hydrothermal stage. The starting gel was prepared as explained in Sections 3.2.1 and 3.2.2 and allowed to age for 24 h. Nickel(II) nitrate hexahydrate (5.8 g) was added to 20 ml of distilled water and stirred vigorously for 0.5 h. This solution was added to the starting gel under stirring at 100°C, until 15 ml water evaporated. The new mixture was then immediately transferred to an oven at 100°C for 48 h. The powders were then filtered, washed and calcined at 550°C for 3 h. The samples are denoted as NaY, $NH_4Y$, CaY, HY, H-USY, and NiY for sodium, $NH_4^+$, $Ca^{2+}$- exchanged, hydrogen, dealumitaed, and Ni-impregnated type Y zeolites, respectively. The sodium silicate and colloidal silica solutions are abbreviated as NS and SS, respectively.

**3.3 Characterization of the zeolites**

Powder x-ray diffraction (XRD) patterns for the synthesized samples were recorded by means of a Siemens D500 diffractometer, with Cu-Kα (λ= 1.5418 Å) radiation at 40 kV and 20 mA in the 2θ range of 10 to 60°. The XRD patterns of the unknown samples were matched to that of the reference crystal structure.

The morphologies and SARs of the powders were observed with scanning electron microscopy (SEM, Philips XL30) with an energy dispersive x-ray spectroscopy (EDX).

Fourier-transformed Infrared (FTIR) spectra were recorded on a Nicolet nexus 470 instrument with a resolution of 0.125 $cm^{-1}$ using the KBr wafer technique.

$^{27}Al$ solid state nuclear magnetic resonance (NMR) spectra were obtained by means of a Bruker AMX300 spectrometer at spinning rate of 5Khz with reference to $Al(NO_3)_3/9H_2O$.

The surface area of the synthesized zeolite particles were measured by means of an ASAP 2020 Brunauer–Emmett–Teller (BET) volumetric area analyzer (ASAP 2020, Micromeritics Instrument Corporation). The pore size distribution of the samples was obtained

by the advanced Barrett–Joyner–Halenda (BJH) method using the adsorption-desorption branches of the isotherms. Prior to these tests, the samples were degassed in a vacuum (10μmHG) at 150°C for 1 h.

## 3.4 Pyrolysis Experiments

### *3.4.1 Sample preparation*

A common type of boundary dam coal was used. The coal sample was characterized according to ASTM Standard Method and Testing. The proximate analysis (ASTM D152) was conducted by means of a NETZSCH TG 209F1 Libra thermogravimetric analyzer unit. The ultimate analysis was performed as per ASTM D3176 by means of a Perkin-Elmer 2400 series II CHNS/O apparatus in order to identify the elements present in the samples.

Proximate and ultimate analyses of this coal are presented in table 3.1. The coal was dried at 80°C for 24h in an oven, and pulverized to the desired particle size of <200μm before being mixed with dried zeolite catalysts to produce samples containing 10 and 20 weight percent catalyst for the TGA experiments. For the pyrolysis experiments conducted in horizontal bench scale reactor experiments, samples containing 10 percent catalyst were used.

**Table 3.1** Proximate and Ultimate Analyses of the boundary dam coal

| **Proximate analysis** | **(wt.%)** |
|---|---|
| Fixed Carbon | 34.63 |
| Volatile Matter | 28.38 |
| Ash | 12.49 |
| Moisture | 24.50 |
| **Ultimate Analysis** | **(wt.%)** |
| Carbon | 58 |
| Hydrogen | 3.38 |
| Nitrogen | 1.81 |
| Sulphur | 1.01 |
| Oxygen* | 23.31 |

*Balance to 100% (100-58(C)-3.38(H)-1.81(N2)-1.01(S)-12.49(Ash)=23.31)

### *3.4.2 Reactor experiment setup*

Catalytic coal pyrolysis experiments were conducted using a bench scale stainless steel horizontal reactor with a 1 inch diameter under a nitrogen stream with a flow rate of 50 ml $min^{-1}$ and using the same heating program as that of the thermogravimetric experiments. Samples with a total weight of 5.55 gr containing 0 and 10 percent catalyst (0.55gr) were prepared. The experiment with no catalyst was carried out using 5 g of coal. A cold trap was used at the outlet of the reactor where condensation of the gasses occurred at 0°C. The remaining uncondensed gasses from the outlet of the cold trap were transferred to and analyzed by an Agilent 490-Micro-

GC system. The solid residue from the reaction and the collected pyrolysis oil were studied by means the mentioned Perkin-Elmer CHNS/O and an Agilent GC-MSD 5973 unit, respectively.

### *3.4.3 Thermogravimetric analysis experiments*

The aforementioned NETZSCH TGA analyzer was used to study the pyrolysis of the boundary dam coal. Before performing kinetics studies, it is of great importance that the reaction is not influenced by the diffusion of reactant gasses to the surface of the particles. According to Zou et al., choosing a sample weight of less than 15mg may result in the elimination of the external and intragranular diffusions [89]. Therefore, 10±2 mg samples were used for the TGA tests. Samples were placed in a ceramic crucible and heated to 200°C at a heat rate of 50K $min^{-1}$ under a nitrogen stream with a flow rate of 20ml $min^{-1}$. The temperature was kept constant for 45 min to ensure complete moisture removal, and was subsequently raised to the final temperature at the same heating rate and remained constant for one hour at that rate. At this point no further evident weight loss was observed. Weight loss of the samples was continuously recorded during the process with a resolution of 0.1µg, and three final temperatures of 500, 550, and 600°C were experimented for each sample. Moreover, each experiment was repeated and average values were used. However, due to the high accuracy of the TGA results, the results of the primary and repeated experiments were almost exactly the same.

Corresponding to the experimental design of the thermogravimetric tests, kinetics study was carried out for the second non-isothermal, and the second isothermal steps of the experiment and kinetics parameters of the catalytic pyrolysis reaction were calculated.

## 3.5 Analysis techniques

In this study, different techniques were used to characterize the synthesized zeolite catalysts and the catalytic coal pyrolysis products. Catalyst characterizations were carried out

employing powder x-ray diffraction (PXRD), scanning electron microscope imaging (SEM), energy dispersive x-ray spectroscopy (EDX), thermogravimetric analysis (TGA), Brunauer-Emmett-Teller (BET), Barrett-Joyner-Halenda (BJH), surface analysis, nuclear magnetic resonance (NMR) and Fourier-transformed infrared spectroscopy (FTIR). Moreover, the catalytic coal pyrolysis experiments were studied employing thermogravimetric analysis (TGA), gas chromatography (GC), gas chromatography–mass spectrometry (GC-MS), and CHNS elemental analysis.

# Chapter Four: **Results and Discussion**

## 4.1 Characterization of zeolite catalysts

Results of the preparation and characterization of the catalysts and pyrolysis experiments are presented in this chapter.

As mentioned before, template-free synthesis and modification of zeolites LTY, LTL and ZSM-5 were desired in this study. Pure zeolite Y was synthesized hydrothermally with two different silica sources and without using any organic SDAs. Parent zeolites were modified using different techniques, including two new techniques for impregnation of the zeolite frameworks with NiO and convenient preparation of dealuminated zeolites. Dealumination of zeolites through this method resulted in partial dealumination of the zeolites through use of a simpler process than the conventional process, which may be complex and requires a continuous flow of steam at high temperatures. However, caution must be exercised when designing the vessel to avoid accidents, due to the high vapor pressure of water at high temperatures. One milliliter of water can produce a theoretical water pressure of 11 bars in a vessel with a volume of 280 ml.

Similarly, LTL and ZSM-5 zeolites were synthesized without any use of organic structure directing agents or templates. Only the hydrogen (acid) forms of these zeolites were characterized and used in the pyrolysis experiments.

### *4.1.1 Powder XRD analysis*

For the PXRD tests, for each sample, a layer of zeolite powder was spread on a zero-background plate and placed in the diffractometer using the specifications mentioned in Chapter Three.

#### 4.1.1.1 XRD patterns of LTY zeolites

The XRD patterns for the two parent type Y zeolites and their corresponding modifications are shown in Figures 4.1 and 4.2. The XRD patterns of the zeolites are in agreement with those of the referenced faujasite linde type Y zeolite presented in Figure 4.3 [90].

The XRD patterns for modified zeolite Y showed slight differences when compared with the parent phase in terms of diffraction intensities, while maintaining the main characteristic peaks. This result suggests the successful exchange of $NH_4^+$, $Ca^{2+}$ and $H^+$ with $Na^+$ in the zeolite framework without causing structural defects. The differences observed between the XRD pattern of the parent and ion-exchanged zeolites may be attributed to the different ionic sizes of the exchanged ions with the original sodium ions. The background of the NiY SS and HY SS zeolites is indicative of the introduction of small amounts of amorphicity, or reduction of crystallinity, due to the impregnation and calcination processes. Moreover, the XRD patterns of the impregnated samples exhibit all the characteristic peaks of the type Y zeolite and suggest that Ni has not been replaced in the T sites of the zeolite frameworks. For the nickel impregnated NiY, the slight reduction in crystallinity may have resulted from the changes in the intermolecular forces, due to the presence of nickel nitrate and/or the sintering of NiO during calcination. However, the patterns matched the reference Y type zeolite XRD patterns, without presenting extra peaks and did not suggest any crystalline transformations.

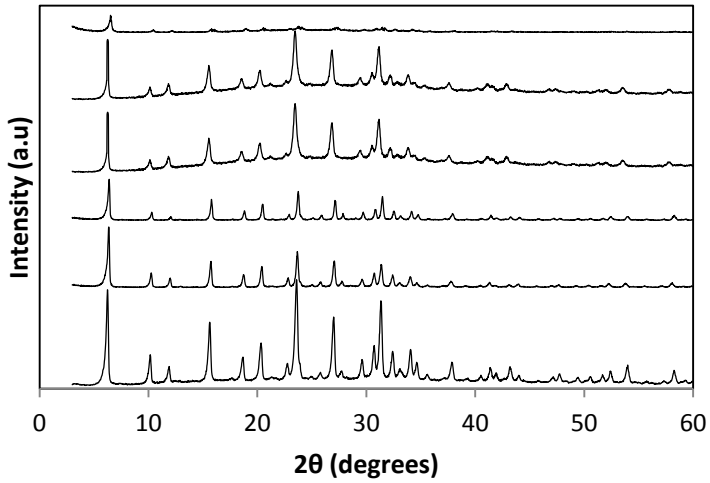


**Figure 4.1** XRD patterns of the samples from parent zeolite Y synthesized with the sodium silicate solution; Patterns from bottom to top are those of NaY NS, $NH_4$Y NS, CaY NS, NiY NS, HY NS and H-USY NS, respectively

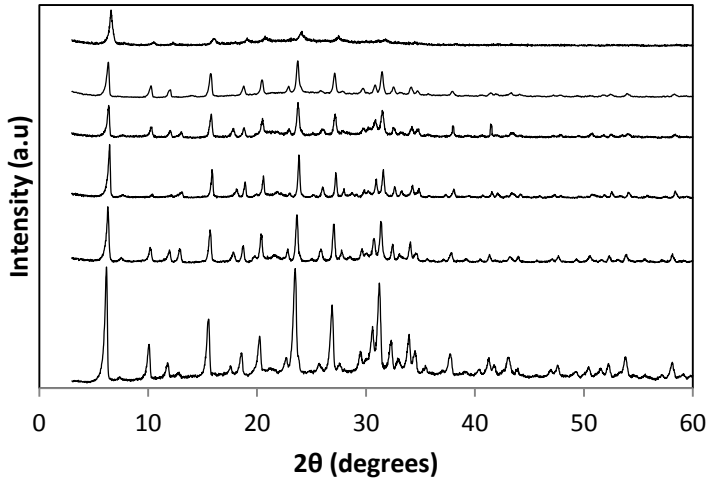


**Figure 4.2** XRD patterns of the samples from parent zeolite Y synthesized with colloidal silica; Patterns from bottom to top are those of NaY SS, $NH_4$Y SS, CaY SS, NiY SS, HY SS and H-USY SS, respectively

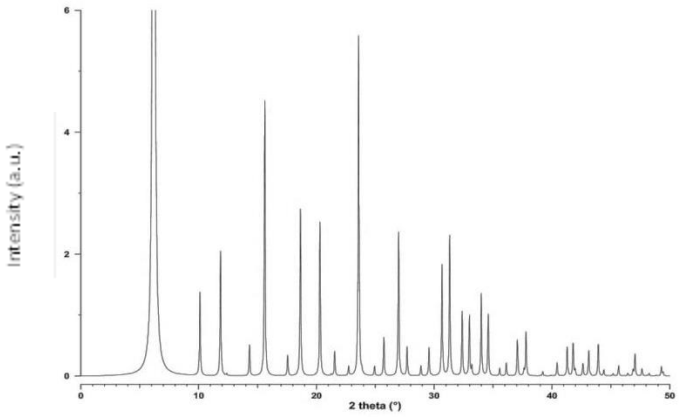


**Figure 4.3** XRD pattern of reference FAU type zeolite [90]

The diffraction intensity decrease was most significant for the dealuminated (H-USY NS) zeolite. The decreased diffraction intensities may be explained by the change of distribution in electron density within the zeolite framework due to the exchange of extra-framework cations with $Na^+$ and the structural changes introduced during the dealumination process.

Comparison of the XRD patterns of the type Y zeolites using the two silica sources showed that the samples synthesized with colloidal silica as a silicon source were less affected by the impregnation and thermal treatment processes, which may be suggestive of higher structural stability of these zeolites.

The nature of the guest molecules and the extent to which these guest molecules fill the pores in the zeolite structure have been observed to affect the distribution of electron density [5, 91].

$H_2O$ molecules are the most common guest molecules that occupy the pores within a zeolite structure. Therefore, to obtain the most accurate XRD results, the samples should be prepared similarly. In this study, all zeolite samples were dried at 100°C in an oven for 5 h and kept outside of the oven overnight at room temperature to obtain hydrated samples without excess amounts of moisture covering the surface of the zeolite.

4.1.1.2 XRD patterns of ZSM-5 zeolites

Synthesis of ZSM-5 usually involves the use of Tetrapropylammonium (TPA), which is an organic structure directing agent or organic template. Given the problems associated with the use of this substance, in this thesis the goal was template-free synthesis of this type of zeolite. The XRD patterns of these zeolites are given in Figures 4.4. The XRD patterns of reference for the ZSM-5 zeolite synthesized using TPA is given in Figure 4.5 [90].

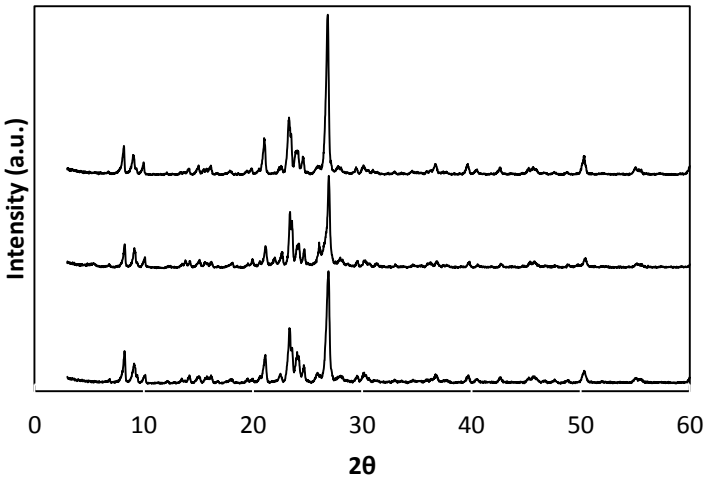


**Figure 4.4** XRD patterns of the ZSM-5 zeolites. Patterns from bottom to top are those of NaZSM-5, $NH_4$ZSM-5, and HZSM-5

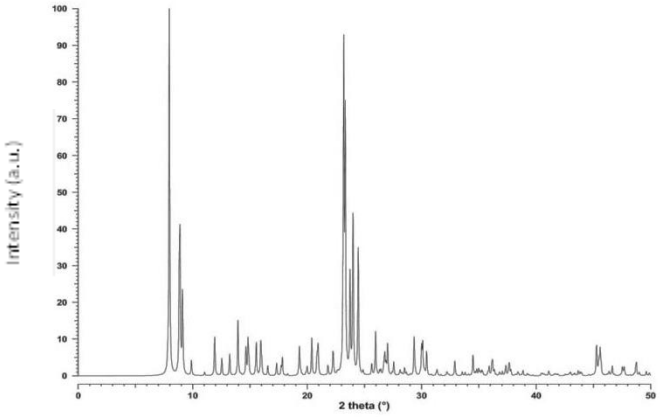


**Figure 4.5** XRD pattern of the reference ZSM-5 zeolite synthesized with the aid of TPA [90]

The patterns showed the characteristic peaks of the ZSM-5 zeolite. Moreover, the slight changes introduced in the patterns due to the modification processes were similar to and in accordance with the changes discussed for type Y zeolites. A few extra peaks were also observed in the patterns of the synthesized ZSM-5 zeolites. These peaks are probably due to the presence of an impurity phase, most likely α-quarts. The peaks at 2θ=20.9° and 26.6° match those for α-quarts [92]. Kulkarni et al. reported the presence of a similar impurity in their work, synthesizing ZSM-5 zeolite using organic templates [93]. They suggested that this phase transformation could be eliminated by reducing the crystallization time. However, in this study, reduction of the crystallization time did not appear to eliminate this impure phase. Moreover, it was found that crystallization times less than 48 h yielded high amounts of amorphous phase. The XRD patterns of the ZSM-5 samples after 18, 24, 36 and 48 h crystallization are presented in Figure 4.6. All synthesis gels were allowed to age for three days.

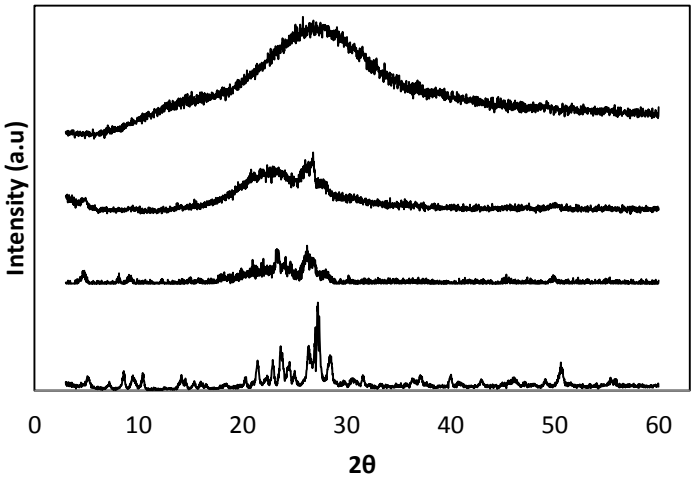


**Figure 4.6** XRD Patterns of ZSM-5 samples after 18, 24, 36 and 48 h of crystallization from top to bottom, respectively

This graph shows that the formation of α-quarts in this method starts almost simultaneously with the ZSM-5 formation. However, comparison of the XRD patterns of the ZSM-5 sample from 48 h of crystallization (Figure 4.6) with that of the sample with 72 h of crystallization (Figure 4.4), is indicative of higher crystallinity in the phases synthesized after 72 h.

4.1.1.3 XRD Patterns of LTL Zeolites

Similar to LTY and ZSM-5 zeolites, XRD patterns of the KLTL and HLTL zeolites were recorded. The XRD patterns of the prepared KLTL zeolites and the reference KLTL zeolites are given in Figures 4.7 and 4.8, respectively.

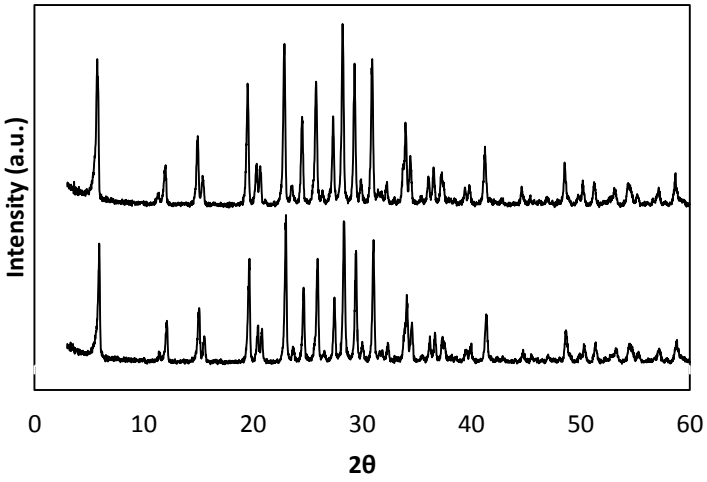


**Figure 4.7** XRD pattern of the KLTL(bottom) and HLTL(top) zeolites

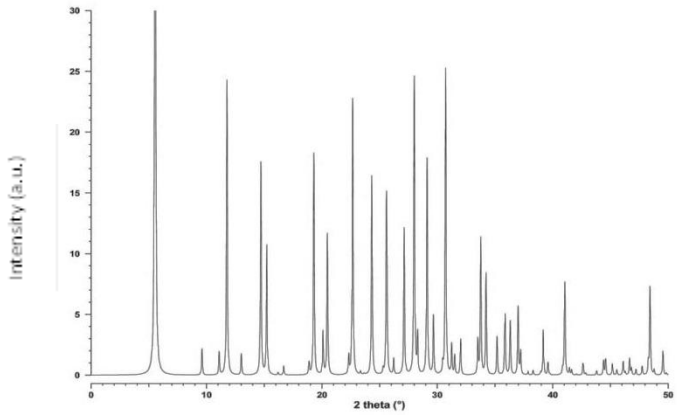


**Figure 4.8** XRD pattern of reference LTL zeolite [90]

No significant changes, other than those already discussed, were observed for this zeolite. The XRD patterns suggest high crystallinity, and no extra peaks suggestive of the presence of impurity phases were observed.

### *4.1.2 Fourier-transformed infrared (FTIR) analysis*

In this research FTIR tests were carried out using the KBr Wafer technique. Five mg of each sample was ground and thoroughly mixed with 200 mg of dry KBr and pressed into a pellet. The KBr Pellet was run on a Nicolet Nexus 470 FT-IR spectrometer, using 16 scans, and scanning from 400 to 4000 $cm^{-1}$. Prior to each run, the FT-IR cell was purged with dry nitrogen.

4.1.2.1 FTIR spectra of LTY zeolites

FTIR analyses were carried out to further study the synthesized zeolites and the changes which occurred due to the modification processes. The reduction of the XRD peak intensities observed for the ion-exchanged LTY zeolites and impregnated samples were not linked to major structural collapses, as shown by Infrared (IR) analyses in Figures 4.9 and 4.10.

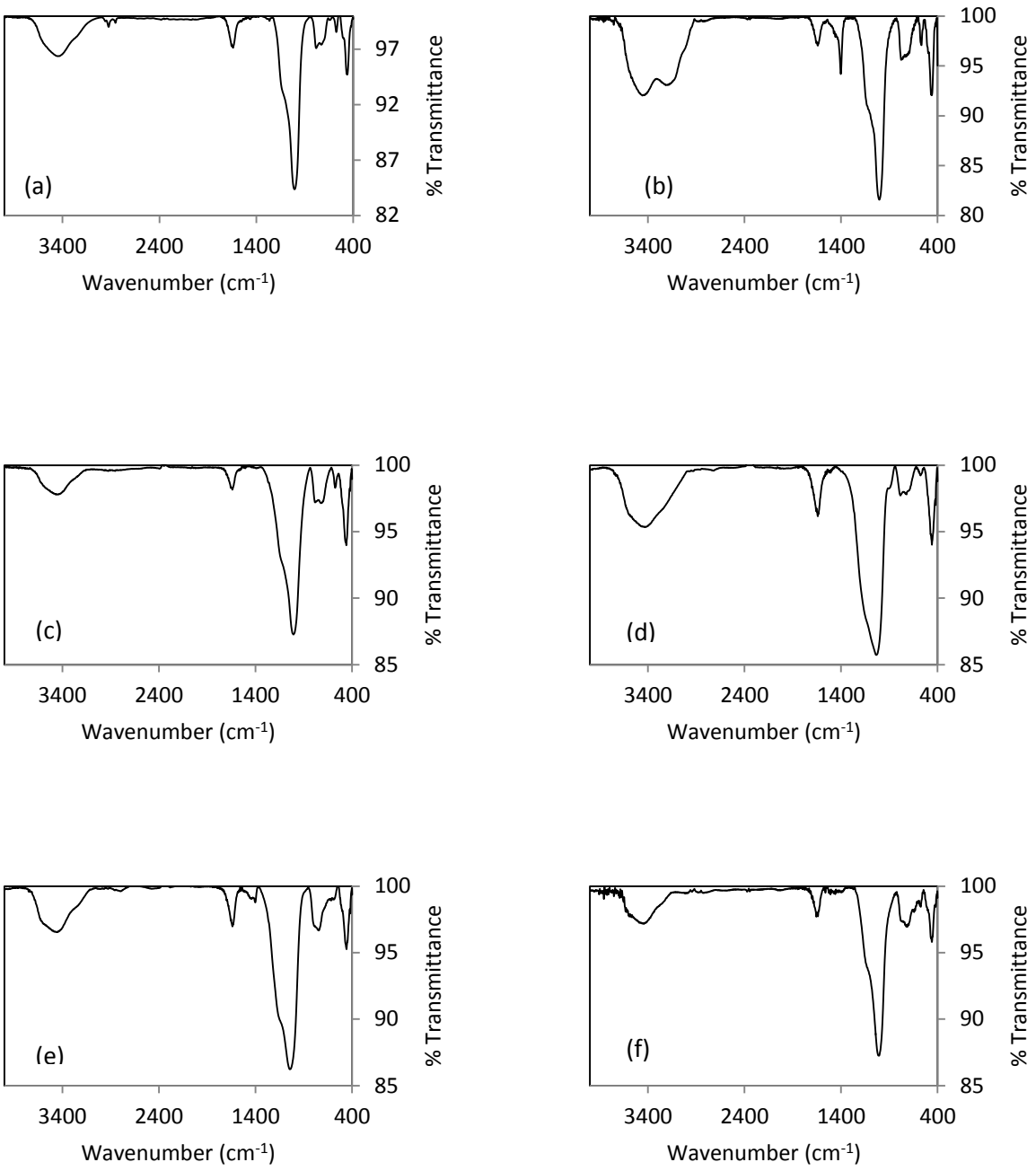


**Figure 4.9** IR Spectra of the original and modified forms of zeolite from colloidal silica:

(a) NaY, (b) $NH_4Y$, (c) CaY, (d) H-Y. (e) H-USY, (f) NiY

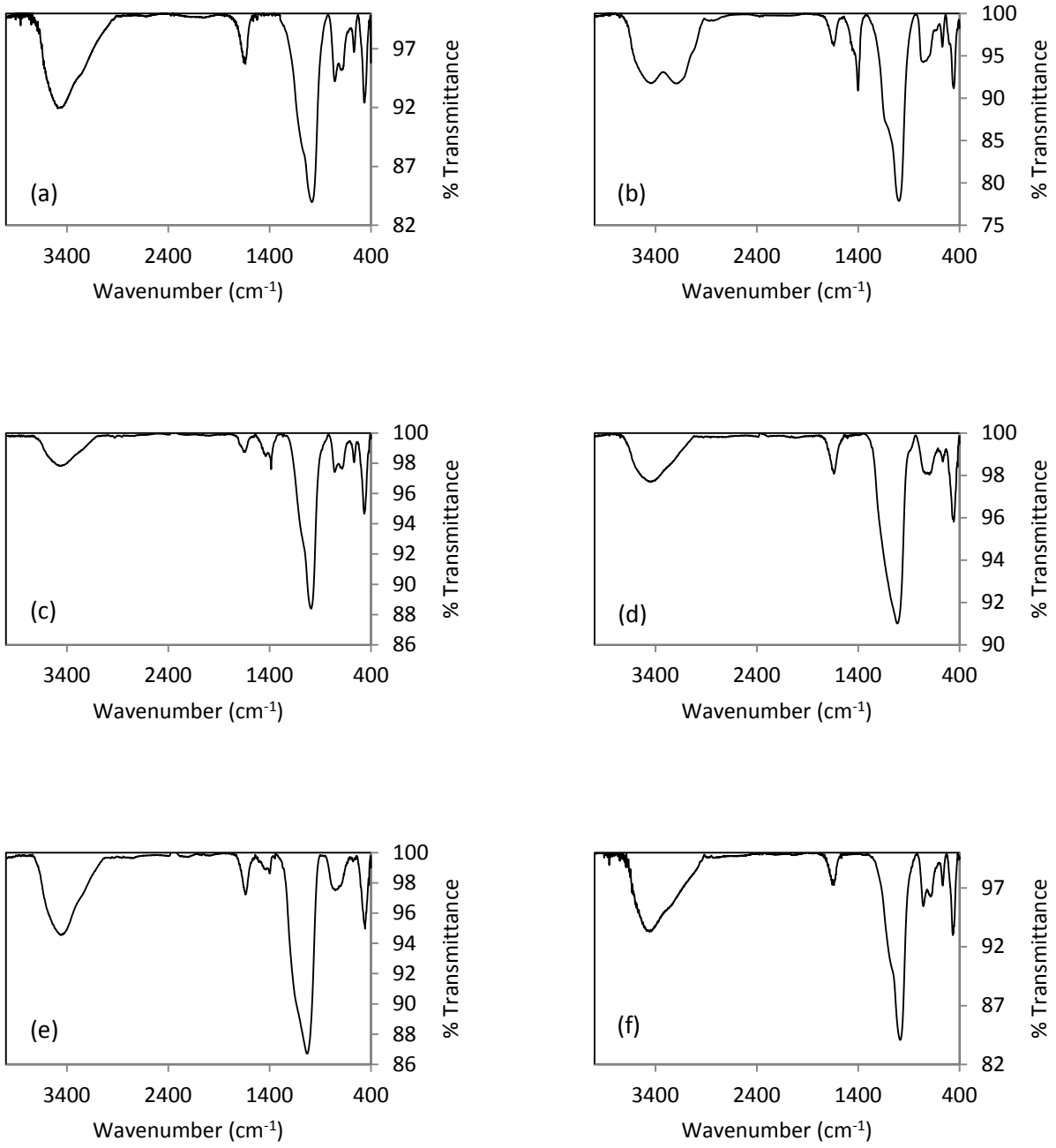


**Figure 4.10** IR Spectra of the original and modified forms of zeolite from sodium silicate:

(a) NaY, (b) $NH_4Y$, (c) CaY, (d) H-Y. (e) H-USY, (f) NiY

IR spectra of the ion-exchanged and impregnated zeolites were very similar to that of NaY and the characteristic bands of the faujasite framework (1004, 780, 575, 450 $cm^{-1}$) [94] were retained with respect to the parent zeolites. Therefore, impregnation and ion-exchange processes did not change the framework structure of the zeolites. The IR spectra showed absorption bands at 950-1250 and 650-720 due to asymmetric and symmetric stretch of internal tetrahedrons, 420-500 $cm^{-1}$ due to T-O bends (T=Si or Al), and 750-820 $cm^{-1}$ due to external linkages. The weak sharp peaks in 1500-1700$cm^{-1}$ correspond to the bending vibration of the water molecules [95]. In the case of the $NH_4$ form and dealuminated zeolites, changes were observed in the hydroxyl group region around 3400 $cm^{-1}$, which were in agreement with the report of Scherzer and Bass [96]. The changes are attributed to the acidic groups [97]. Moreover, the presence of a band around 1400 $cm^{-1}$ associated with the N-H bond vibrations [98] may be indicative of incomplete deammoniation which in turn may explain the mediocre SAR ratio increase in the H-USY zeolites and why the treatment process did not result in significant structural damage.

4.1.2.2 FTIR spectra of ZSM-5 zeolites

The FTIR spectra of the ZSM-5 zeolite samples are given in Figure 4.11. The IR spectra of these samples showed the characteristic adsorption bands corresponding to those from the literature [98]. Bands at 920-1250 $cm^{-1}$ and 1050-1150 $cm^{-1}$, due to internal symmetric and asymmetrical stretches, and bands at 500-650 $cm^{-1}$, due to ring vibrations, and bands at 420-500 $cm^{-1}$due to T-O bends were clearly observed and were in accordance with the band assignments reported in the literature [99]. However, the extra peaks observed in the fingerprint region of the spectrum are probably due to the slight crystalline changes, different extra-framework cations, and presence of α-quartz. Furthermore, similar to the $NH_4$ form derivatives of zeolite Y, the small peak at ca. 1400 observed in the IR spectrum of the prepared HZSM-5 sample is indicative

of the remaining N-H bonds from the untransformed $NH_4^+$ ions. The appearance of a new peak at the hydroxyl region corresponding to the presence of OH groups was also in agreement with the reports in literature [99].

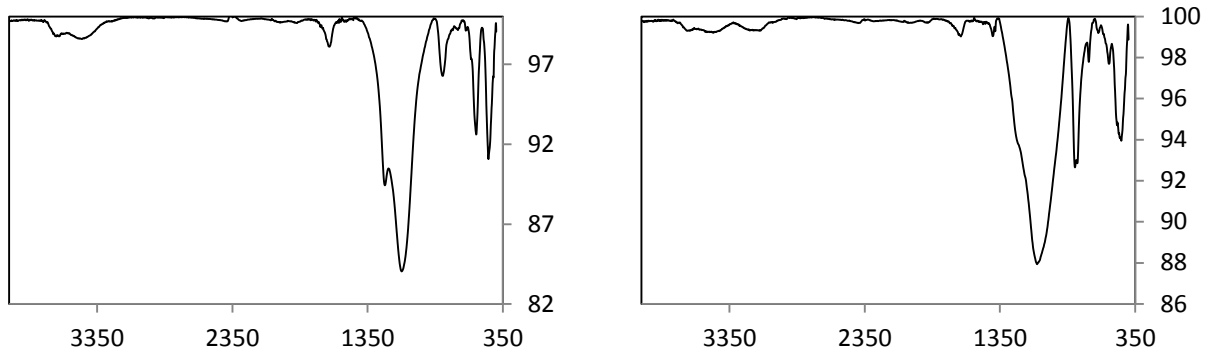


**Figure 4.11** IR spectra of the NaZSM-5(left) and HZSM-5(right) samples

4.1.2.3 FTIR spectra of LTL Zeolites

IR spectra of LTL zeolites are given in Figure 4.12. The bands of the IR spectra of these samples are in agreement with those reported in the literature by Pichat et al. [98].

The spectra show bands at 1000-1200 $cm^{-1}$, due to asymmetric stretch of tetrahedra, and bands at ca. 770 $cm^{-1}$ and 725 $cm^{-1}$,indicative of symmetric stretch of O-(Al,Si)-O and $AlO_4$ tetrahedra, and bands at ca. 608 and 477 $cm^{-1}$, related to the vibration of the double-six-rings and bending vibrations of O-(Al,Si)-O bonds, and bands at ca. 1650 $cm^{-1}$, which were attributed to the bending vibration of water. Moreover, the bands at 438 $cm^{-1}$, due to the vibrations of the 12-ring pores, were evident in both IR spectra.

Similar changes to the hydrogen forms of LTY and ZSM-5 zeolites were observed in the hydroxyl region of the IR spectrum of the HLTL zeolite, due to the acidity caused by the presence of acidic groups. Furthermore, the absence of the adsorption band at ca.1400 $cm^{-1}$ of the

IR spectrum of the HLTL zeolite is indicative of rather complete deammoniation of the ammonia ions.

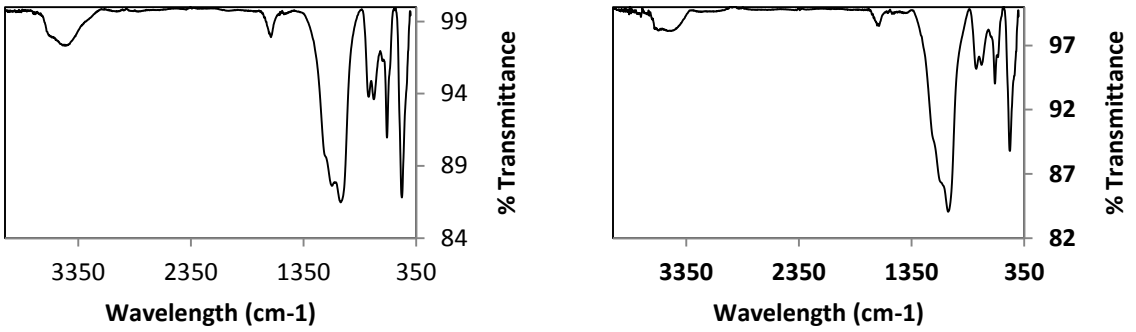


**Figure 4.12** IR spectra of the KLTL (left) and HLTL (right) samples

### *4.1.3 Solid State Nuclear Magnetic Resonance (NMR) analysis of the dealuminated type Y zeolites*

Aluminum (Al) coordination of the dealuminated type Y zeolite samples was examined by $^{27}$Al solid state NMR spectrometry. Due to the limitations for using the spectrometer, and the fact that NMR spectroscopy could give the most informative results for the dealuminated samples, the NMR spectroscopy tests were only performed for these samples. The NMR spectra of these samples are given in Figure 4.13.

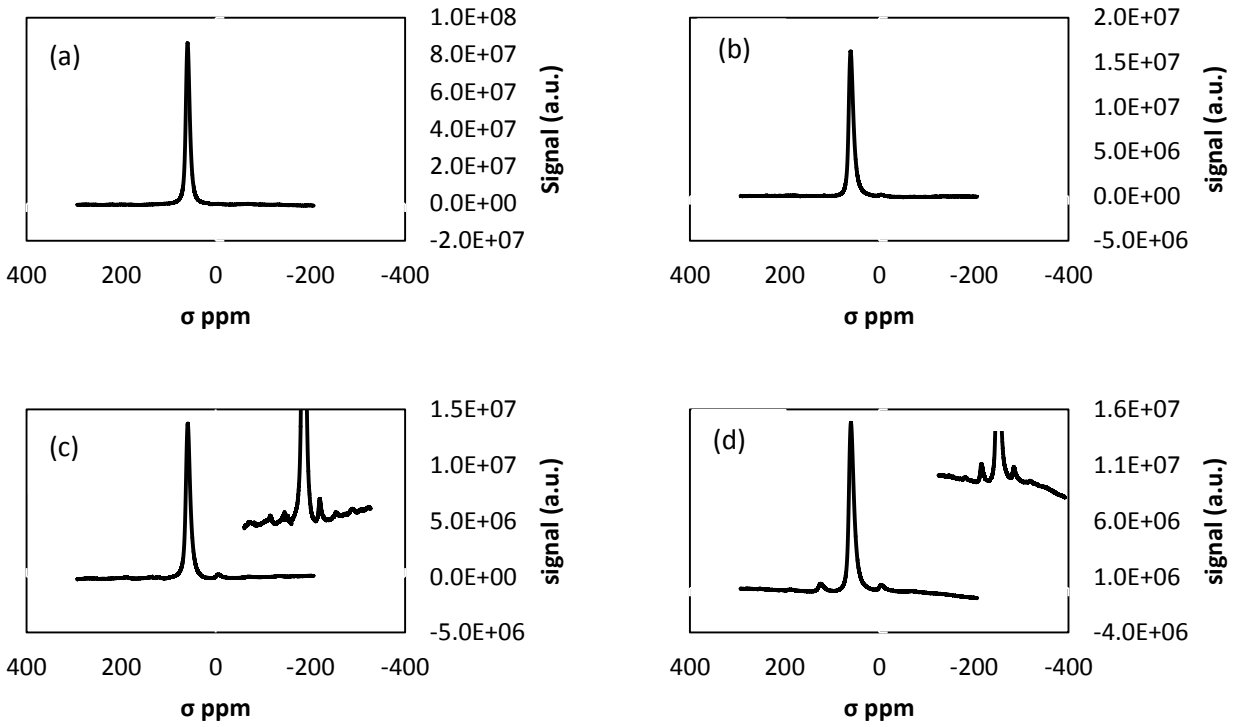


**Figure 4.13** $^{27}$Al solid state NMR spectra of the parent and ultrastable (dealuminated) zeolites; (a)NaY SS (b)NaY NS (c)H-USY SS (d)H-USY NS

$^{27}$Al spectra of the NaY zeolites consist of a single sharp signal at ca. 60 ppm that is representative of tetrahedrally coordinated Al in the zeolite framework. Appearance of the peaks at ca. 0 ppm after hydrothermal treatment is associated with the octahedrally coordinated non-framework aluminum species. The intensity decrease of the tetrahedrally coordinated Al signals observed with the appearance of the non-framework Al signals was in agreement with the reports in literature [100-101]. The spectrum of the H-USY NS contains an extra peak at ca. 120 ppm, presumably due to some impurity. Moreover, due to the small intensity of the non-framework Al signals, the originality of the peaks appearing at ca. 0 ppm was tested by repeating the NMR tests

at different spinning rates. Small intensity of the non-framework Al signals is representative of partial dealumination of the samples.

### *4.1.4 Scanning Electron Microscopy (SEM), and Energy-dispersive X-ray spectroscopy (EDS, EDX, or XEDS)*

4.1.4.1 SEM and EDX analysis of LTY Zeolites

The EDX analyses were carried out to determine the Si/Al ratio (SAR) of the samples. The results of the EDX analyses are given in Table 4.1. The SARs measured with EDX were 2.25-2.8 and 1.67-2.05 for the samples prepared with the colloidal silica and sodium silicate solution as the silicon source, respectively. Compared with the SARs of the modified and parent zeolites, the H-USY (dealuminated) zeolites showed a higher SAR, but no other significant changes were found. However, the effect of the ion-exchange processes and instrument error may explain the small differences in the SARs of the parent and ion-exchanged zeolites. The ion-exchange process had almost no effect on the zeolite SAR, but the high temperature (550°C) and the accompanying high pressure may have resulted in dissolution of aluminum during the preparation of the H-USY sample, resulting in a higher SAR, as explained in Chapter Two.

**Table 4.1** EDX results of the samples prepared with two silica sources. (NS and SS represent sodium silicate and silica solution respectively)

| Zeolite | O | Na | Al | Si | Ni | Ca | N | Si/Al | $SiO_2/Al_2O_3$ |
|---|---|---|---|---|---|---|---|---|---|
| NaY NS | 35.94 | 13.1 | 19.05 | 31.9 | - | - | - | 1.67 | 3.34 |
| $NH_4$Y NS | 45.55 | 4.26 | 12.3 | 20.85 | - | - | 17.04 | 1.66 | 3.33 |
| CaY NS | 48.94 | 5.23 | 14.34 | 24.86 | - | 6.64 | - | 1.73 | 3.46 |
| H-Y NS | 46.31 | 12.41 | 15.53 | 25.75 | - | - | - | 1.66 | 3.32 |
| H-USY NS | 45.55 | 3.26 | 16.82 | 34.37 | - | - | - | 2.04 | 4.08 |
| NiY NS | 42.13 | 17.94 | 14.32 | 24.12 | 1.49 | - | - | 1.68 | 3.36 |
| NaY SS | 36.79 | 12.02 | 15.69 | 35.5 | - | - | - | 2.26 | 4.52 |
| $NH_4$YSS | 52.21 | 3.96 | 5.2 | 12.16 | - | - | 26.37 | 2.33 | 4.67 |
| CaY SS | 51.71 | 2.26 | 12.13 | 28.4 | - | 7.49 | - | 2.34 | 4.68 |
| H-Y SS | 29.72 | 10.75 | 18.24 | 41.29 | - | - | - | 2.26 | 4.52 |
| H-USY SS | 47.78 | 1.95 | 12.95 | 36.33 | - | - | - | 2.80 | 5.61 |
| NiY SS | 40.06 | 11.03 | 12.67 | 33.3 | 2.93 | - | - | 2.62 | 5.25 |

The SEM images of the zeolite powders are shown in Figures 4.14 and 4.15. These images show fine particle sizes between 500 nm and 2 μm for the samples synthesized using the sodium silicate solution as the silica source and between 500 nm and 1.5 μm for those produced using the colloidal silica.

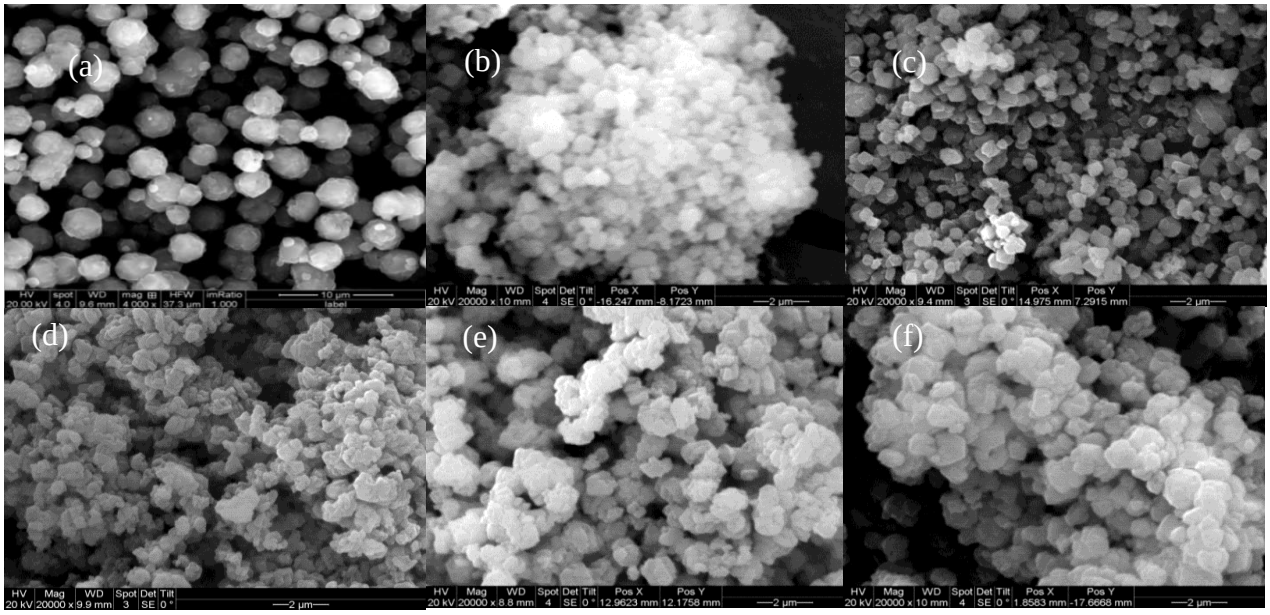


**Figure 4.14** SEM images of the parent zeolite synthesized with sodium silicate as the silicon source: (a) NaY, (b) $NH_4Y$, (c) CaY, (d) HY, (e) NiY, (f) H-USY

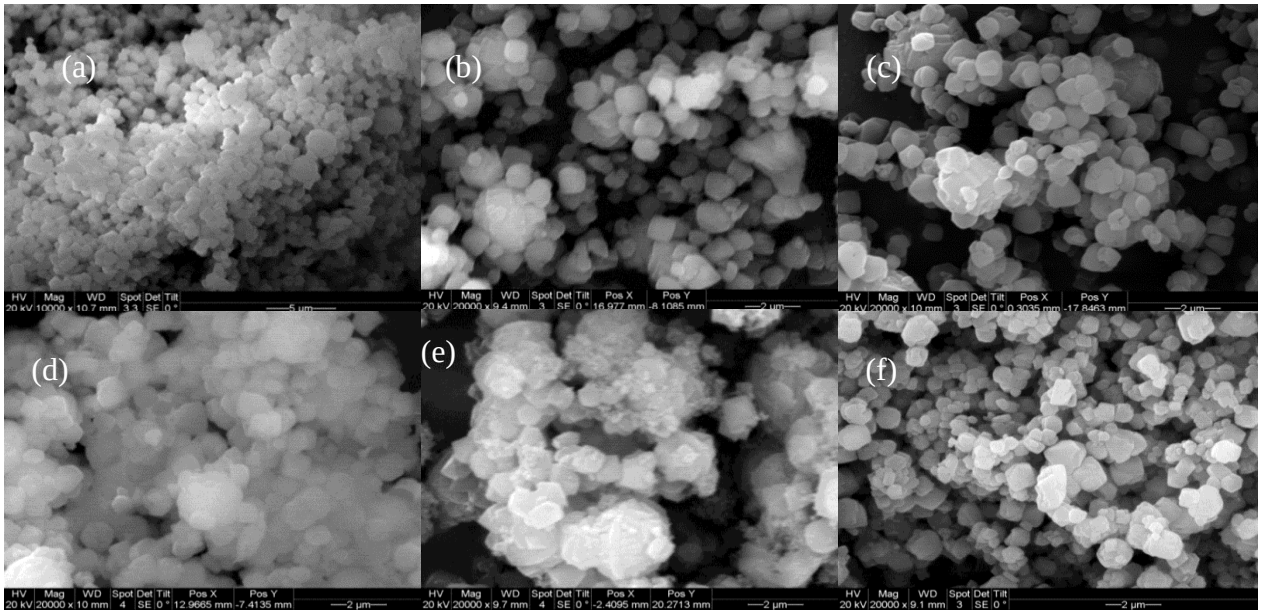


**Figure 4.15** SEM images of the parent zeolite synthesized with colloidal silica as silicon source: (a) NaY, (b) $NH_4Y$, (c) CaY, (d) HY, (e) NiY, (f) H-USY

The composition of the aqueous solution (Si, Al and Na concentrations), the nature of the raw materials, the pH and hydrothermal temperature are all important synthesis parameters which affect the nucleation rate, crystal formation, yield, size, and type of the zeolite particles. However, because of the differences in the synthesis gels in this study, it is difficult to evaluate the dependency of the crystallinity and crystal sizes of the prepared zeolites on the silica sources.

Furthermore, it can be seen that the morphology of the samples did not show a dramatic change in most samples. A slight deformity was introduced in the nickel impregnated samples, which can be explained by the sintering of metal oxides. Nearly all metal oxides are affected by sintering, which is related to the coalescence and growth of the oxide crystallites. Sintering may result in a decrease in the pore openings, with the possibility of pores being blocked completely. This phenomenon also explains the severe decrease in the BET surface of the nickel impregnated samples. Moreover, the acidic nature of the nickel nitrate solution added to the synthesis gel and pH decrease may also explain the observed changes.

Dealumination through steaming at high temperatures may cause framework defects, local structure collapse, or even blocking of some channels. From the SEM images, it can be seen that the dealuminated samples had largely retained their form even after being modified and calcined at high temperatures.

#### 4.1.4.2 SEM and EDX analysis of ZSM-5 Zeolites

SEM images of the ZSM-5 samples are given in Figure 4.16.

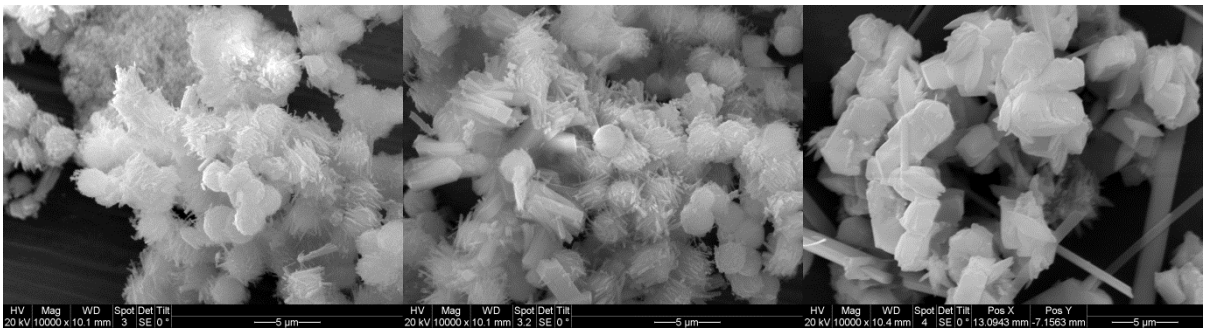

**Figure 4.16** SEM images of the NaZSM-5(left), $NH_4$ZSM-5(middle), and H-ZSM-5(right) samples

The SEM images of the three investigated ZSM-5 zeolites were very similar to each other. Moreover, two types of morphologies and particle sizes ranging from 2 to 4 microns were observed. EDX analysis performed on both morphologies observed suggested similar molar compositions. This suggests that the different morphologies can have similar structures while appearing differently under the microscope, due to different arrangement of the particles of similar structure. Moreover, the morphologies observed in the SEM images of the samples are consistent with those reported by Zhang et al. [102] Unreacted silica species were sporadically observed, and EDX was carried out to confirm their nature. The EDX analysis results of the ZSM-5 samples are given in Table 4.2.

**Table 4.2** EDX analysis result for the ZSM-5 samples

| Zeolite | O | Na | Al | Si | N | Si/Al | $SiO_2/Al_2O_3$ |
|---|---|---|---|---|---|---|---|
| NaZSM-5 | 42.29 | 2.20 | 3.38 | 52.12 | - | 15.42 | 30.84 |
| $NH_4$ZSM-5 | 34.11 | 1.27 | 3.43 | 54.84 | 6.35 | 15.98 | 31.97 |
| HZSM-5 | 40.72 | 0.53 | 3.78 | 54.96 | - | 14.53 | 29.08 |

The variations observed in the SAR of the ZSM-5 zeolite samples could be explained by unreacted materials and impurity phases in the sample. Synthesis of the ZSM-5 zeolites with higher SARs using $TPA^+$ has been reported in the literature [93].

4.1.4.3 SEM and EDX analysis of LTL Zeolites

The SEM images of the LTL type zeolites are given in Figure 4.17.

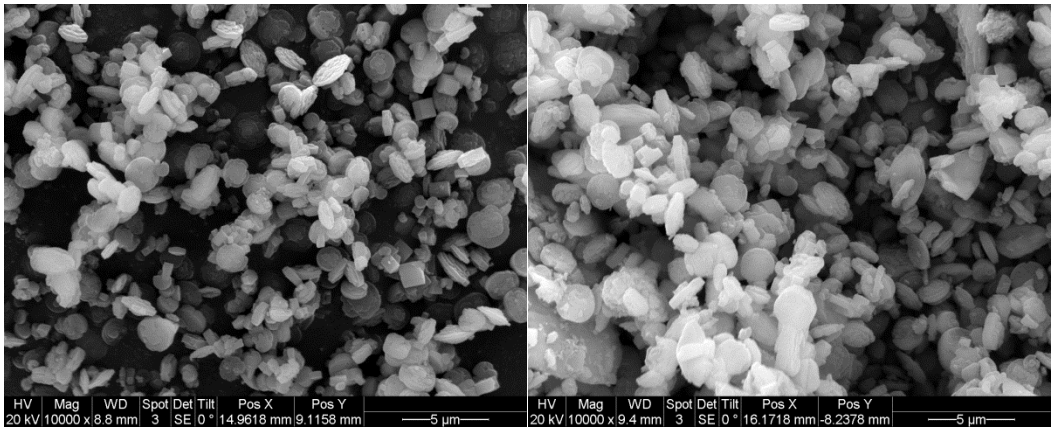


**Figure 4.17** SEM images of the KLTL (left) and HLTL (right) sample

The SEM images of the LTL type zeolites showed excellent uniformity, both with regard to particle size distribution and morphology, and particle sizes ranging between 2 and 3 microns are dominantly seen. Moreover, the SAR of the prepared LTL type zeolite samples were determined by the means of EDX analysis. The EDX analysis for the LTL type sample is given in Table 4.3.

**Table 4.3** EDX analysis result for the LTL samples

| Zeolite | O | K | Al | Si | Si/Al | $SiO_2/Al_2O_3$ |
|---|---|---|---|---|---|---|
| KLTL | 53.81 | 10.94 | 8.05 | 27.20 | 3.38 | 6.76 |
| HLTL | 55.13 | 7.86 | 8.47 | 28.54 | 3.36 | 6.73 |

### *4.1.5 BET surface area analysis*

In this study, the calculations for the surface area analysis were performed by the ASAP 2020 software provided by Micromeritics. Samples were degased for 45 min in vacuum before analysis.

4.1.5.1 Surface area analysis of type Y zeolites

Surface area analysis was conducted and the resultant BET surface area of the parent and modified zeolites (with an error of ±5$m^2$/g) is presented in Table 4.4.

**Table 4.4** Results of the surface area analysis of the samples

| **Zeolite** | **BET Surface Area ($m^2$/g)** | **Micropore Area ($m^2$/g)** |
|---|---|---|
| NaY NS | 645 | 590 |
| $NH_4$Y NS | 503 | 443 |
| CaY NS | 498 | 451 |
| HY NS | 403 | 235 |
| H-USY NS | 491 | 418 |
| NiY NS | 321 | 285 |
| NaY SS | 656 | 610 |
| $NH_4$Y SS | 542 | 461 |
| CaY SS | 547 | 493 |
| HY SS | 437 | 386 |
| H-USY SS | 523 | 510 |
| NiY SS | 363 | 320 |

Parent zeolite Y with a high specific surface area was fabricated from both silicon sources. After ion exchange, the number, size and position of the substituted cations affect the pore size of the zeolite. Consequently, ion exchange of the original sodium extra- framework cations resulted in the decrease in specific surface area and the micropore area of all samples. Although the ion-exchange process had only a slight influence on the SAR (*c.f.* Table 4.1), it induced microstructural change to some extent. For instance, local three-dimensional porous structures may have collapsed during this process, resulting in lower specific surface area.

A more significant decrease was observed in the case of nickel impregnated samples. This difference can be explained by the metal oxide sintering phenomenon or slight morphology changes due to the different pH of the synthesis gel of these zeolites.

All the parent and modified zeolite Y samples prepared from the colloidal silica exhibited higher specific surface areas than those from the sodium silicate solution, which was probably due to their overall smaller particle size (Figures 4.14 and 4.15).

The pore size distribution of the parent and modified zeolite Y samples prepared from both silicon sources was obtained from BJH analysis and results are shown in Figures 4.18 and 4.19.

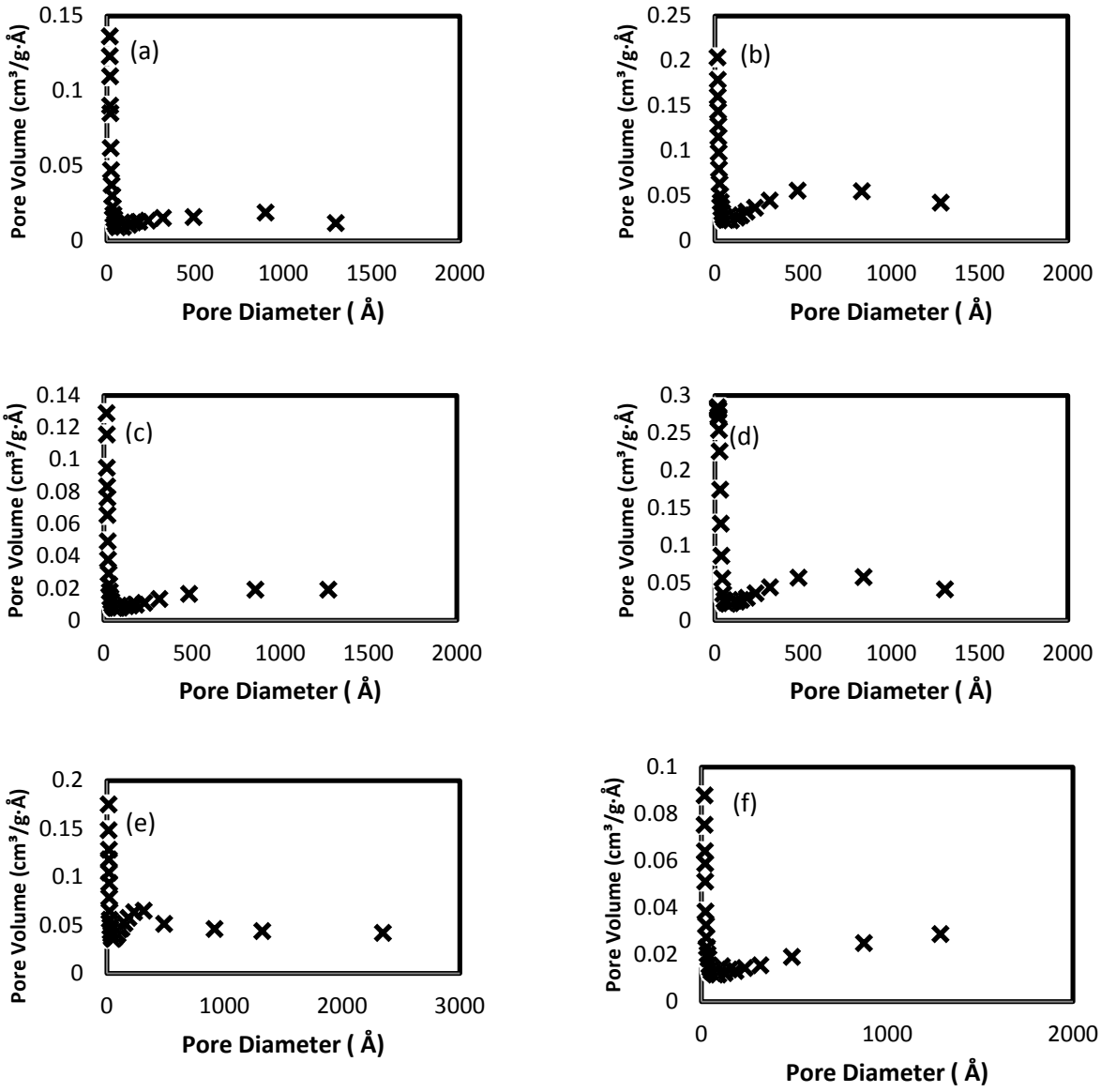


**Figure 4.18** BJH pore size distribution graphs of the original and modified forms of zeolite from sodium silicate: (a) NaY, (b) $NH_4Y$, (c) CaY, (d) H-Y. (e) H-USY, (f) NiY

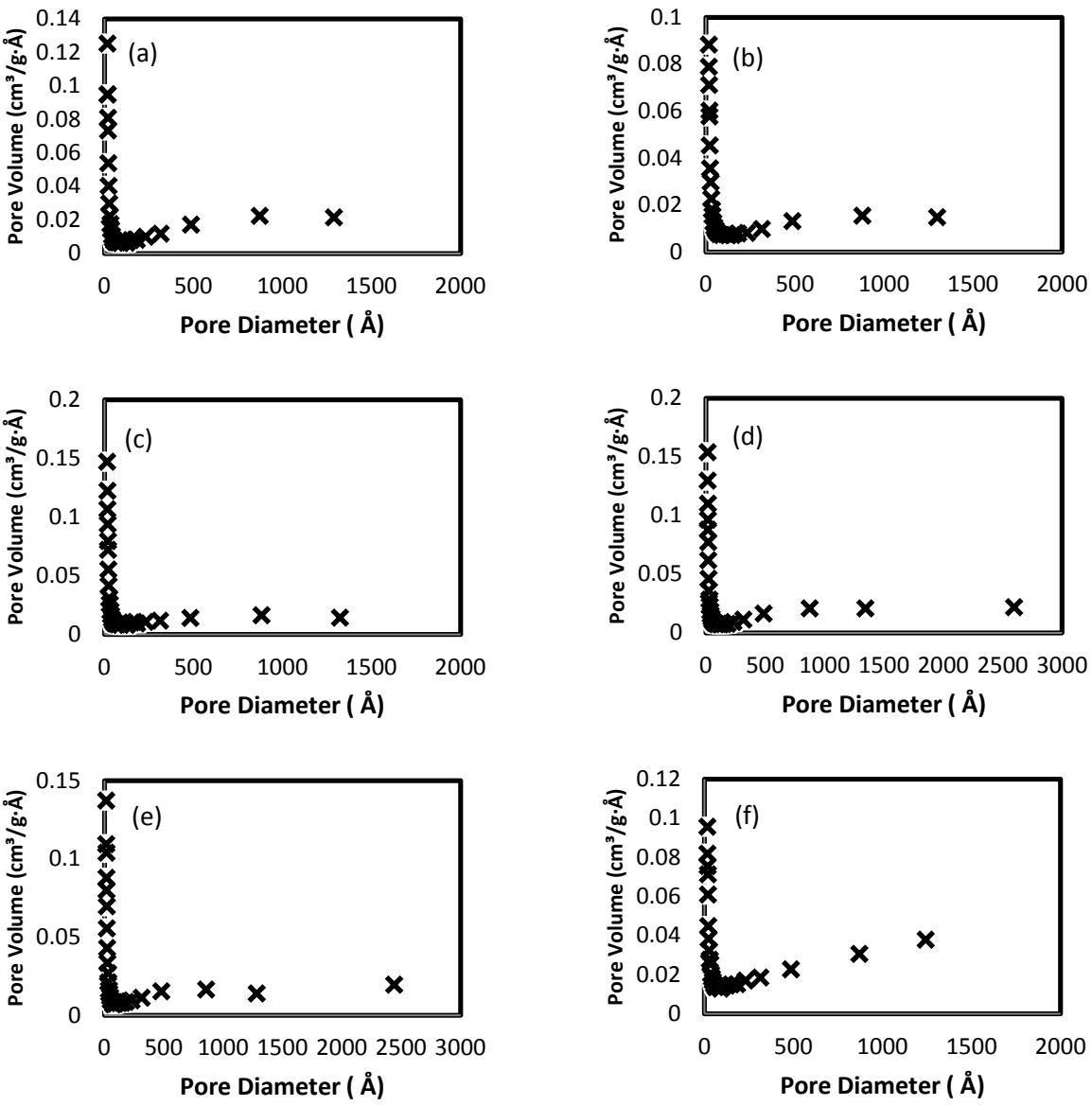


**Figure 4.19** BJH pore size distribution graphs of the original and modified forms of zeolite from silica solution: (a) NaY, (b) $NH_4Y$, (c) CaY, (d) H-Y. (e) H-USY. (f) NiY

No obvious differences in the pore size distribution could be readily found for all the samples, irrespective of silicon sources. All of them demonstrated microporosity, as evidenced from the sharp semi-peak around 2 nm. Careful analysis reveals that a different mode existed in

the modified samples, with a higher proportion of larger pores. Nevertheless, the majority of the pores were smaller than 20 nm, and larger-sized pores constituted only a small portion. The differences observed in the case of nickel impregnated samples may be indicative of slight pore size irregularity introduced to the structure due to the impregnation process or the NiO sintering and blockage of some pores.

4.1.5.2 Surface area analysis of type ZSM-5 Zeolites

Results of the surface area analysis conducted on the ZSM-5 samples are given in Table 4.5.

**Table 4.5** Surface area analysis results of the LTL type samples

| Zeolite | BET Surface Area ($m^2/g$) | Micropore Area ($m^2/g$) |
|---|---|---|
| NaZSM-5 | 145.9 | 110.2 |
| H-ZSM5 | 132.1 | 99.9 |

Similar to the changes observed for type Y zeolites, a reduction in the BET surface area seemed to have occurred in the thermal treatment of the NaZSM-5 sample. These changes can be attributed to similar phenomena outlined for the type Y zeolites.

Furthermore, BJH analysis results were recorded, and pore size distributions were obtained. The obtained BJH graphs are presented in Figure 4.20.

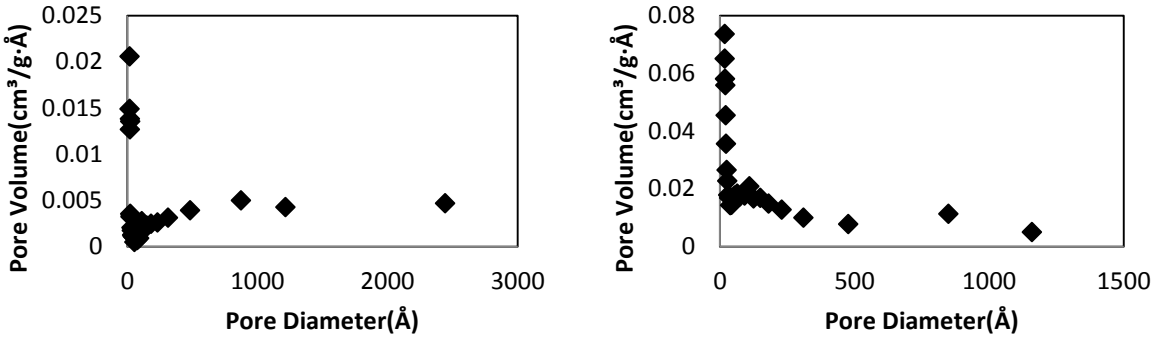


**Figure 4.20** BJH pore size distribution graphs of NaZSM-5(left) and H-ZSM-5(right)

Similar to type Y zeolite samples, the sharp peak around 2 nm is indicative of the microporosity of these samples. The mode in the NaZSM-5 diagram seems to have shifted to the left after the thermal treatment. This change may be due to the smaller size of hydrogen ions, some pore size irregularity introduced to the sample due to the thermal treatment or the incomplete deammoniation and the existence of $NH_4^+$ ions in some pores.

4.1.5.3 Surface area analysis of type LTL Zeolites

Results of the surface area analysis conducted on the LTL samples are given in Table 4.6.

**Table 4.6** Surface area analysis results of the LTL type samples

| Zeolite | BET Surface Area ($m^2/g$) | Micropore Area ($m^2/g$) |
|---|---|---|
| KLTL | 210.8 | 189.1 |
| HLTL | 170.4 | 158.7 |

Surface area measurements for the LTL type zeolites showed a similar downward trend as those of type Y and ZSM-5 zeolites, which could be explained based on similar principles and phenomena outlined for zeolite Y and ZSM-5. Similar changes were also evident in the BJH pore

size distribution diagrams. The pore size distribution graphs for these graphs are presented in Figure 4.21.

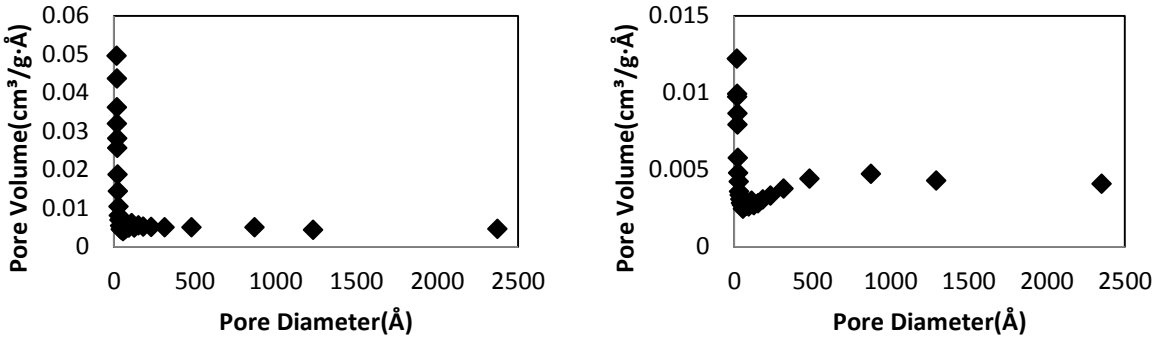


**Figure 4.21** BJH pore size distribution graphs of KLTL(left) and HLTL(right)

## 4.2 Pyrolysis

Results of the catalytic coal pyrolysis experiments that were carried out, as explained in Chapter 2, are presented in this chapter.

### *4.2.1 Gas chromatography (GC) analysis*

4.2.1.1 GC analysis of experiments with type Y (NS) zeolite catalysts

The effect of catalyst additives on the evolution of $H_2$, $CH_4$, CO, and $CO_2$ gases in the catalytic pyrolysis of the boundary dam coal was investigated using a bench scale horizontal reactor, as explained in Chapter Two, under nitrogen atmosphere and a heating rate of 50 K/min. Results of the GC analysis of the produced gases in the experiments employing (NS) type Y zeolites as catalysts are demonstrated in Figure 4.22. The GC measurements were carried out every four minutes and the connection of the points on the graphs is only for a better visual representation. The pyrolysis reactions consisted of four stages. Water vapor is usually considered the only gas release attributed to temperatures lower than 200°C for all types of coals,

which was covered in the first two stages of the pyrolysis reactions in this study. No detectable amounts of the mentioned gases evolved until the end of the first isothermal step (under 200°C), which was assumed to be the beginning of the pyrolysis reaction. The third stage was the non-isothermal pyrolysis of coal, where the temperature increased from 200°C to 600°C. CO and $CO_2$ were the first gases that evolved between 200 and 400°C, which may indicate that they come from the same reaction process [103]. At these temperatures several processes, such as disruption of hydrogen bonds, vaporization, and breakage of other non-covalent bonds take place [104]. Methane rapidly started to release at temperatures higher than 450°C, which is close to the results found by Arenillas for anthracite and bituminous coals [105]. The evolution of $H_2$ commenced at around 450°C. The maximum concentration recorded for the released $H_2$ gas was lower in comparison to the other measured gases, and the H-ZY catalyst seemed to have decreased the $H_2$ formation. Considering the work of Serio et al. [108], the release of $H_2$ can be attributed to the breakage of the bonds during the pyrolysis between 500 and 600°C. Evolution of the gases was fastest and reached a maximum in the first few minutes of the second isothermal step (600°C), and quickly decreased afterwards.

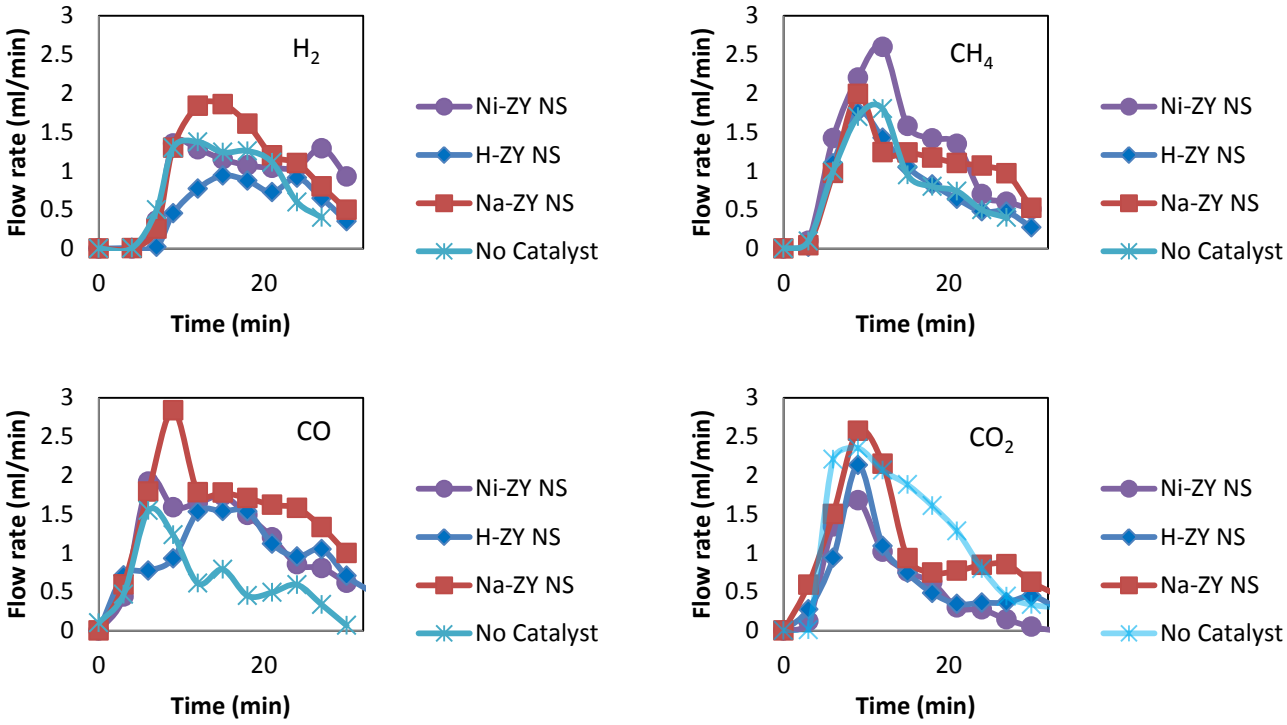


**Figure 4.22** Evolution of gas species during the catalytic coal pyrolysis experiments by NS type Y zeolite catalysts

Generally, all NS type Y zeolite catalysts promoted the evolution of CO gas and hindered $CO_2$ production. Higher amounts of $H_2$ and CO were generated in the samples with NaY NS, and samples containing Ni-ZY NS produced the highest $CH_4$. CO is one of the products of many decomposition reactions, such as oxygen-containing heterocyclic compounds and is also a product of the reaction of $CO_2$ with char at high temperatures, which are both possible sources of the produced CO in the experiments [106]. Generally, all NS type Y zeolites seem to have promoted the release of CO and $CH_4$ during the reaction. The exact mechanism of methane formation during the coal pyrolysis reaction is still unknown. However, Solomon and Hamblen

proposed that methane is produced from methoxy and methyl groups attached to aromatic rings [107-108].

4.2.1.2 GC analysis of experiments with type Y (SS) zeolite catalysts

Gas chromatography (GC) results for the catalytic coal pyrolysis reactions using the type Y zeolites synthesized with colloidal silica as the silicon source are given in Figure 4.23. Similar to NS type Y zeolites, CO and $CO_2$ were the first gases detected by the micro GC. From visual comparison of the graphs, it can be seen that the overall production of CO has not changed significantly in the experiments with SS type Y zeolites. The SS type Y zeolite graphs for CO show less significant difference compared to the graph of the experiment with no catalyst, than when compared with the NS type Y zeolites, and the maximum CO flow rate recorded is lower than that recorded for the NS type Y zeolites. The graphs of $CO_2$ evolution were also significantly different from those of NS type Y zeolites. The SS type catalysts seem to have reduced the $CO_2$ generation more effectively than the NS type catalysts. Furthermore, unlike the NS type Y zeolites, all of the SS type Y zeolites seem to have increased the $H_2$ generation. Moreover, theses catalysts, excluding the H-ZY SS catalyst, increased the $CH_4$ generation. It can also be seen that both NS and SS Nickel impregnated type Y zeolites promoted higher $CH_4$ concentrations. However, the NaY SS catalyst seems to have comparably increased the $CH_4$ generation.

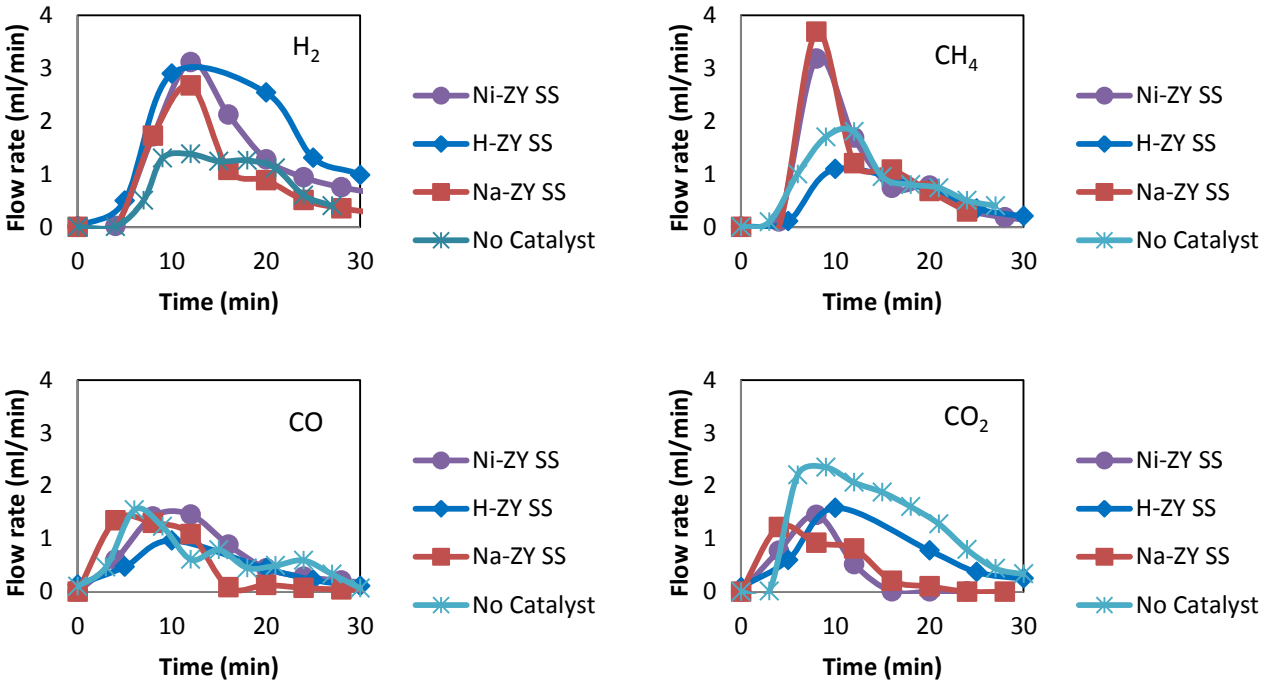


**Figure 4.23** Evolution of gas species during the catalytic coal pyrolysis experiments by the SS type Y zeolite catalysts

4.2.1.3 GC analysis of experiments with of ZSM-5 zeolite catalysts

The GC results recorded for the experiments using ZSM-5 zeolites are presented in the diagrams of Figure 4.24. It can be seen that the generation of $H_2$, $CH_4$, and $CO_2$ gases in the experiments with ZSM-5 has decreased. However, the production of CO has increased. The presence of a catalyst can promote the production of new compounds by facilitating reactions such as hydrogenation, dehydrogenation, isomerization, etc. Unfortunately, the available Micro GC was only able to measure the four mentioned gases. Therefore, it is difficult to draw further conclusions from the GC diagrams.

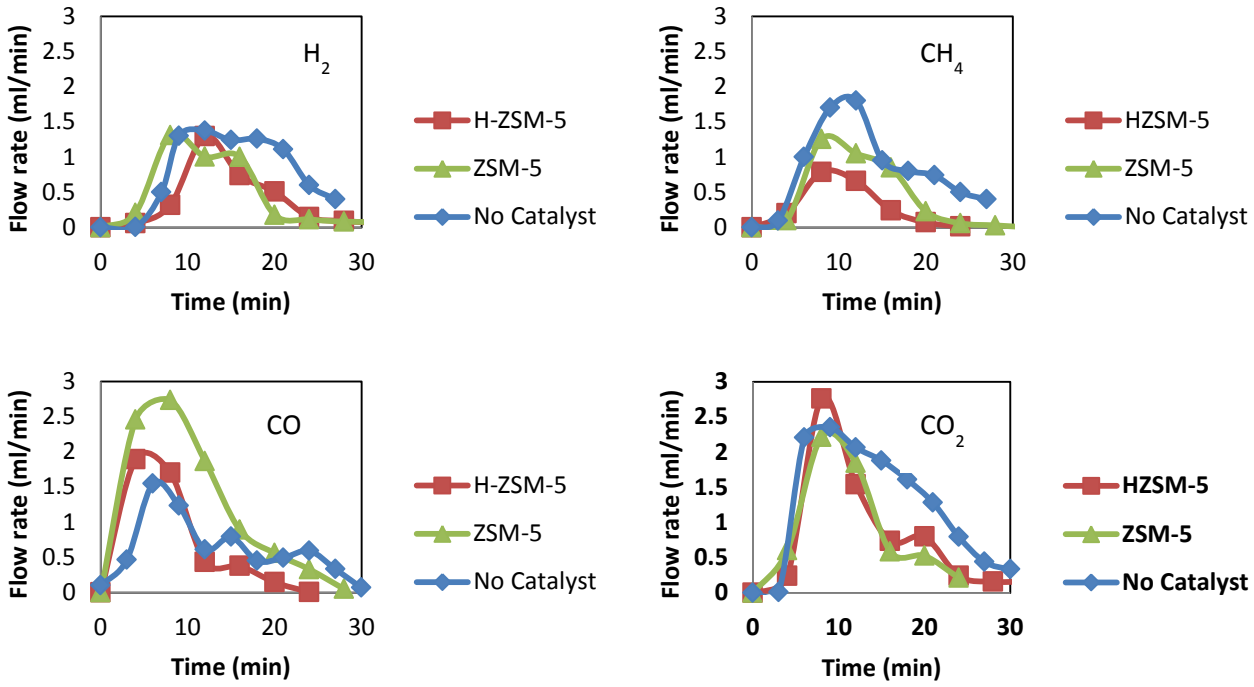


**Figure 4.24** Evolution of gas species during the catalytic coal pyrolysis experiments by the ZSM-5 type catalysts

4.2.1.4 GC analysis of LTL Zeolites

The GC results for the experiments with LTL zeolites are presented in Figure 4.25. Similar changes to those observed for the $H_2$ gas in the ZSM-5 experiments were observed for the experiments with LTL zeolites. Less CO and $CO_2$ gases seemed to have been produced in the experiments with LTL zeolites. However, the changes in the $CH_4$ production were not significant when compared to the experiment with no catalyst.

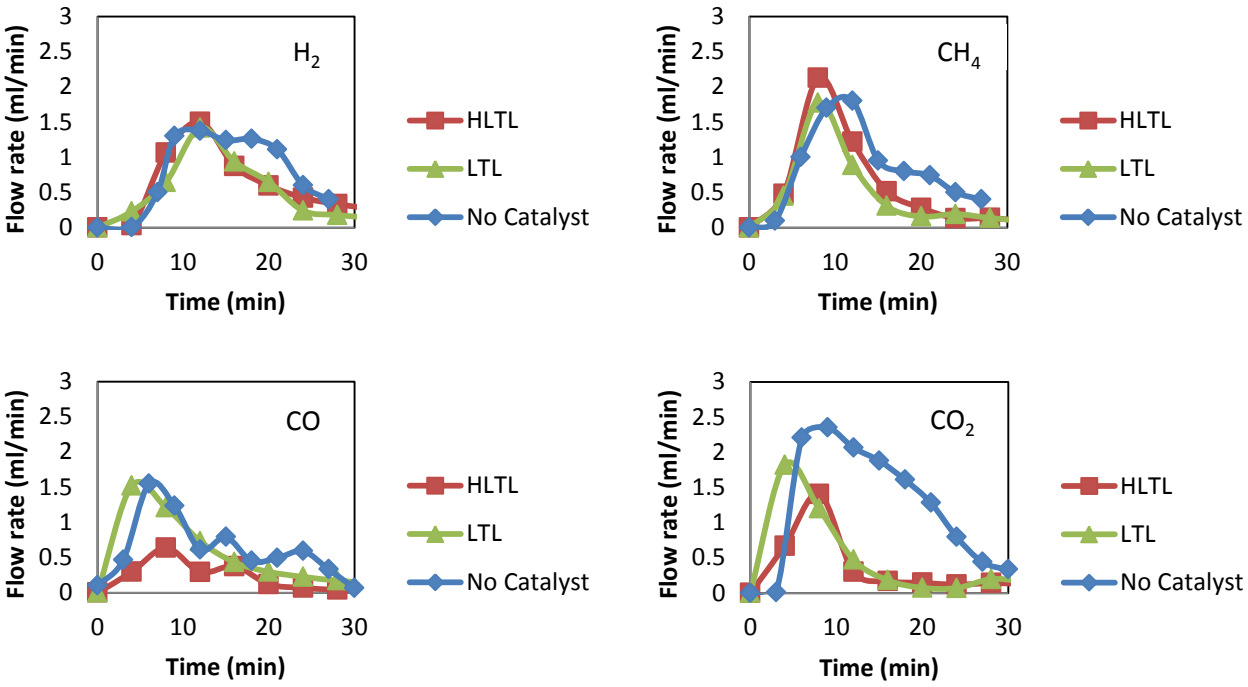


**Figure 4.25** Evolution of gas species during the catalytic coal pyrolysis experiments by the LTL type zeolite catalysts

As mentioned previously, the use of catalysts may significantly change the gaseous and liquid products of the pyrolysis reaction. Due to the limited capability of the used Micro GC in measuring the gases, further analysis of the effects of the catalysts was not possible.

### *4.2.2 Elemental analysis of the solid and liquid products*

4.2.2.1 Solid and liquid residues of experiments with NS and SS type Y zeolite catalysts

A complex mixture of condensable hydrocarbons, including aromatic and other oxygen-containing hydrocarbons, are released during the pyrolysis process at temperatures between 400 and 600°C [109]. It is very difficult to measure these condensates due to the complexity of the reactions and the presence of water. However, the total weight of the condensed liquids from the catalytic coal pyrolysis experiments obtained using a cold trap at 0°C were measured in this study. The weight of the liquids obtained from the catalyst-free sample, and samples with NaY,

H-ZY and Ni-ZY NS catalysts were 0.6, 0.6, 0.4, and 0.8 g respectively. The amount of liquid product obtained from each SS type zeolite was almost equal to the amount obtained with its NS type counterpart. Na-Y catalysts did not influence the amount of the obtained liquid. Less liquid was condensed using the H-ZY catalysts, which may be indicative of the production of lighter compounds with lower condensation temperatures. Use of the Ni-ZY catalysts increased the liquid by about 30 percent, which is suggestive of a high distribution controlling effect of this catalyst.

Furthermore, 3.52, 3.56, 3.48, and 3.49 g of solid residues were obtained from the pyrolysis experiments of the raw coal sample, and samples with NaY, H-ZY, and Ni-ZY NS catalysts, respectively, which were only slightly different. The weights of the solid residues obtained from experiments with SS type zeolites were only slightly less than those obtained from the experiments with the NS type catalysts.

Ultimate analyses of the liquid and solid residues from the pyrolysis experiments were performed using the mentioned CHNS/O analyzer, and the results are shown in Tables 4.7 and 4.8. All solid residue samples have higher carbon and lower sulfur contents and, therefore, production of char or coke, which is a cleaner coal, is one the main goals of coal pyrolysis.

**Table 4.7** CHNS/O analysis results for the solid residue of the pyrolysis experiments with type Y catalysts

| Sample | No catalyst | NaY NS | H-ZY NS | Ni-ZY NS | NaY SS | H-ZY SS | Ni-ZY SS |
|---|---|---|---|---|---|---|---|
| C | 68.23 | 67.03 | 64.28 | 69.59 | 67.76 | 63.65 | 64.36 |
| H | 3.25 | 1.61 | 1.45 | 1.34 | 1.57 | 1.34 | 1.39 |
| N | 1.76 | 1.54 | 2.09 | 2.06 | 2.16 | 1.81 | 2.64 |
| S | 0.56 | 0.55 | 0.4 | 0.39 | 0.4 | 0.47 | 0.42 |
| O* | 13.71 | 16.78 | 19.3 | 14.13 | 15.62 | 20.24 | 18.7 |

*balanced to 100% considering 12.49% ash content

In comparison with the coke produced from the raw coal, all NS catalysts reduced the hydrogen, and sulfur content of the produced cokes in the order of Ni-ZY>H-ZY>NaY, which may suggest higher production of hydrogen and sulfur containing compounds in gaseous product in similar order. The oxygen contents reported in this study are merely the result of balancing the measurements to 100%. Nitrogen contents changed in a different pattern. The nitrogen content was increased by H-ZY NS and Ni-ZY NS catalysts, but decreased by NaY NS, which suggests that, as opposed to H-ZY NS and Ni-ZY NS, the NaY NS catalyst may promote new reactions in which nitrogen participates.

Analysis of the coke residues obtained with the SS type Y zeolite catalysts was considerably different and the amounts of nitrogen and sulfur changed differently. The changes may be attributed to the utilization of the different catalysts but no conclusions could be readily drawn from their variation.

**Table 4.8** CHNS/O analysis results for the liquid residue of the pyrolysis experiments with type Y catalysts

| Sample | No catalyst | NaY | H-ZY | Ni-ZY | NaY SS | H-ZY SS | Ni-ZY SS |
|---|---|---|---|---|---|---|---|
| C | 4.49 | 4.76 | 4.3 | 3.84 | 4.63 | 5.48 | 4.32 |
| H | 11.65 | 11.59 | 11.09 | 15.66 | 11.35 | 15.68 | 15.94 |
| N | 0.94 | 1.44 | 2.48 | 1.76 | 0.97 | 2.78 | 1.68 |
| S | 2.3 | 2.22 | 2.5 | 2.98 | 2.12 | 2.9 | 3.06 |

No regular patterns were observed in the elemental analysis of the liquid residues except for nitrogen and sulfur. These results emphasized the different catalytic and distribution controlling effects of the catalysts. All catalysts increased the nitrogen content of the liquids and sulfur was only reduced insignificantly in the case of the Na-Y catalysts. Moreover, due to the probable presence of water in the liquid samples, the oxygen balance was not carried out for these samples.

4.2.2.2 Solid and liquid residues of experiments with LTL and ZSM-5 zeolite catalysts

The CHNS analysis of the solid and liquid products of the pyrolysis experiments with the LTL and ZSM-5 catalysts is given in Tables 4.9 and 4.10.

**Table 4.9** CHNS/O analysis results for the solid residue of the pyrolysis experiments with LTL and ZSM-5 catalysts

| Sample | No catalyst | ZSM-5 | H-ZSM-5 | LTL | HLTL |
|---|---|---|---|---|---|
| C | 68.23 | 66.04 | 61.41 | 62.41 | 62.73 |
| H | 2.25 | 1.76 | 1.72 | 1.84 | 1.63 |
| N | 1.76 | 2.12 | 1.94 | 1.44 | 1.83 |
| S | 0.56 | 0.42 | 0.48 | 0.46 | 0.47 |
| O* | 14.71 | 17.17 | 21.96 | 21.36 | 20.85 |

*balanced to 100% considering 12.49% ash

**Table 4.10** CHNS/O analysis results for the liquid residue of the pyrolysis experiments with LTL and ZSM-5 catalysts.

| Sample | No catalyst | ZSM-5 | H-ZSM-5 | LTL | HLTL |
|---|---|---|---|---|---|
| C | 4.49 | 2.48 | 3.65 | 3.72 | 3.43 |
| H | 11.65 | 12.69 | 12.47 | 12.72 | 12.53 |
| N | 0.94 | 1.62 | 1.52 | 1.44 | 1.83 |
| S | 2.3 | 2.26 | 2.26 | 2.15 | 2.24 |

Similar to the experiments with type Y zeolites, no significant fluctuation can be observed in the analyses of the solid or liquid samples from the experiments with LTL and ZSM-5. The liquid sample obtained when the ZSM-5 catalyst was used had the lowest carbon content among all samples which may suggest higher production of light hydrocarbons in the gaseous product.

Furthermore, similar trends were observed in the analyses of the liquid samples from these experiments with regards to hydrogen, nitrogen and sulfur.

### *4.2.3 GC-MS Results; All Catalysts*

The liquid products from these experiments were obtained by condensing the gaseous products in a cold trap at 0°C. The liquid samples obtained were analyzed by GC-MS. The GC-MS results for NS and SS type Y zeolites are given in Table 4.11.

**Table 4.11** The results of GC-MS tests for all catalysts

| Component | No Catalyst (mol %) | ZY NS | ZY SS | HZY NS | HZY SS | NiZY NS | NiZY SS | ZSM-5 | H-ZSM-5 | LTL | H-LTL |
|---|---|---|---|---|---|---|---|---|---|---|---|
| Manganese(II) acetate | 0.03 | 0.31 | 0.06 | 0.06 | 0.06 | 0.08 | 0.13 | 1.33 | 0.45 | - | - |
| 2-Pentanone, 4-hydroxy-4-methyl- | - | - | 0.11 | - | 0.12 | - | 0.17 | - | - | - | - |
| Toluene | 3.04 | 0.55 | | 1.38 | - | - | - | - | - | 1.24 | 5.35 |
| Furan, tetrahydro-3-methyl- | - | - | - | - | - | 3.08 | 0.14 | - | - | 1.32 | |
| (2,3-Dimethyloxiranyl)methanol | 0.03 | 0.19 | 0.04 | 0.05 | 0.04 | 0.08 | - | 1.11 | 0.39 | - | - |
| 5-Hepten-2-one | 1.02 | 0.10 | 6.57 | | 0.03 | | 0.91 | 0.72 | 0.25 | - | - |
| Furan, 2,5-dihydro-2,5-dimethyl- | - | - | - | 0.92 | 1.20 | - | 0.40 | 0.08 | 0.14 | - | - |
| 2-Pentene, 4,4-dimethyl- | 1.10 | - | 0.04 | 0.12 | 0.09 | 8.70 | 13.98 | 0.40 | 0.17 | - | - |
| 2-Pentanone, 4-hydroxy-4-methyl | 0.76 | 4.21 | 8.23 | 5.02 | 5.73 | - | 0.36 | 9.38 | 2.12 | - | - |
| 2-Propanone, 1-(dimethylamino)- | - | 4.08 | 18.43 | 4.26 | 15.58 | - | 4.25 | 0.64 | - | - | - |
| p-Xylene | - | 1.36 | 0.6 | - | - | 2.43 | 0.75 | - | - | 2.02 | 0.05 |
| o-Xylene | 0.09 | - | - | 0.98 | - | - | 0.16 | - | - | 1.33 | - |
| Benzene, 1,3-dimethyl- | 0.06 | 0.18 | 0.21 | 0.53 | 0.11 | - | - | - | - | - | - |
| Butanedial | - | - | 0.09 | - | 0.11 | - | 0.70 | - | - | - | - |
| Benzene, 1-ethyl-3-methyl- | 0.06 | - | - | 0.31 | - | 16.43 | 14.13 | - | - | 0.94 | - |
| Pyrrole, 1-methyl-3-(1,1-dimethylethyl)- | - | 0.88 | 0.21 | 0.10 | 0.53 | - | 1.78 | - | - | - | - |
| Phenol | - | - | 1.95 | 0.85 | 4.63 | 11.93 | 9.04 | 42.15 | 39.32 | 38.15 | 52.41 |
| Benzene, 1-ethyl-2-methyl- | 0.23 | - | 4.23 | 0.72 | 2.37 | 9.06 | 25.43 | 15.77 | - | 6.51 | 7.30 |
| 2-Hydrazino-6-methyl-pyrimidin-4-ol | - | 0.15 | - | - | 1.72 | 1.05 | 0.59 | 7.51 | 6.41 | 5.07 | 7.69 |

**Table 4.12** (4.11 continued) The results of GC-MS tests for all catalysts

| Component | No Catalyst (mol %) | ZY NS | ZY SS | HZY NS | HZY SS | NiZY NS | NiZY SS | ZSM-5 | H-ZSM-5 | LTL | H-LTL |
|---|---|---|---|---|---|---|---|---|---|---|---|
| 2-Hexanone, 6-(acetyloxy)- | - | - | 15.94 | - | 16.62 | 2.74 | - | 18.86 | 5.74 | - | - |
| Benzene, 1,3,5-trimethyl- | 0.17 | - | 0.22 | 0.31 | 0.24 | 5.62 | 3.41 | - | 2.29 | - | - |
| Benzene, 1,2,3-trimethyl- | - | - | - | - | - | 1.85 | 3.83 | - | - | 1.52 | - |
| Phenol, 2-methyl- | 0.10 | - | 0.16 | 0.35 | 0.33 | - | 0.82 | 0.74 | 6.24 | - | - |
| Naphthalene | 0.04 | - | 3.05 | 0.15 | 1.76 | 10.89 | 5.08 | 0.21 | 2.13 | 9.178 | - |
| Cyclohexanone, 2-propyl | - | - | 1.24 | 0.39 | 1.98 | 7.45 | - | - | - | 10.162 | - |
| Phenol, 4-methyl- | - | - | - | - | - | 4.94 | - | - | - | 3.466 | 7.72 |
| 1H-Indene, 3-methyl- | 0.15 | 0.14 | 0.44 | 0.22 | 2.49 | - | - | - | 3.31 | - | - |
| Phenol, 2-methyl- | - | - | - | - | - | 2.48 | - | 1.08 | 5.57 | 2.317 | 3.73 |
| 4-Piperidinone, 2,2,6,6-tetramethyl- | 0.54 | 0.58 | 12.57 | 1.74 | 11.28 | - | - | 1.10 | 1.33 | 1.545 | - |
| Phenol, 3,4-dimethyl- | - | - | - | - | - | - | - | 0.13 | 3.01 | 1.53 | - |
| Undecane, 2,3-dimethyl- | - | 0.19 | - | - | 0.17 | - | - | - | - | 1.51 | - |
| Naphthalene | 5.34 | - | - | - | - | 7.89 | - | - | - | 3.58 | - |
| Naphthalene, 2-methyl- | 0.80 | 0.86 | - | - | - | 0.92 | - | - | - | 1.07 | - |
| 1H-Indene, 1-ethylidene- | 0.60 | 0.49 | - | 0.84 | - | - | - | - | - | 0.82 | - |
| Naphthalene, 2,6-dimethyl- | 0.86 | - | - | 0.37 | - | - | - | - | - | - | - |
| Naphthalene, 2,3-dimethyl- | 0.19 | 0.34 | - | - | - | - | - | - | - | - | - |
| Naphthalene, 1,3-dimethyl- | 0.28 | 0.78 | - | 0.36 | - | - | - | - | - | - | - |
| 3,4-Hexanedione, 2,2,5-trimethyl- | - | 0.33 | - | 0.06 | - | - | - | - | - | - | - |
| Naphthalene, 2,3,6-trimethyl- | - | - | - | - | - | 1.47 | - | - | - | 2.89 | - |

The results of the GC-MS tests showed the catalysts are able to promote the production of certain compounds such as 4,4-dimethyl-2-Pentene, 4-hydroxy-4-methyl-2-Pentanone (Diacetone alcohol),1-(dimethylamino)-2-Propanone (N,N-Dimethylisopropanolamine), 1-ethyl-3-methyl-Benzene(3-Ethyltoluene),1-ethyl-2-methyl-Benzene (2-Ethyltoluene),Phenol, 4-methyl-phenol (p-Cresol), Naphthalene, 6-(acetyloxy)-2-Hexanone, 2-propyl-cyclohexanone.

Many variations were observed in the concentrations of the compounds in the liquid products. These variations can be attributed to the effect of the catalysts on the mechanism of the reactions as well as the selectivity provided by them. The porous structure and pore size of the zeolites were discussed earlier in this chapter. Sometimes the pores of zeolites admit small molecules but prevent large ones from entering. Therefore, zeolites are also known as molecular sieves. The pores can control the residence time of various molecules in the vicinity of the catalytically active surface to an extent that allows only certain molecules to react. One example of high selectivity of zeolite catalysts is the formation of xylene from toluene and methane [110].

Theoretically, methane and toluene enter through the pore opening and react on the interior surface of type Y zeolites. Ortho, para and meta xylenes are the products of this reaction. However, due to the pore size of the zeolite only para-xylene can exit. Therefore, a high selectivity for para-xylene is observed. In this study, such selectivity can be seen in the results of the experiments with sodium form and nickel impregnated type Y zeolites. Another feature of the zeolite catalysts is controlled placement of the reacting molecules by the catalyst atoms. For instance, the formation of benzene molecules from ethane molecules may be facilitated by this phenomenon [111].

The different types of zeolite catalysts used in this study have different structures and pore sizes. Investigation of the exact mechanisms occurring in the reactions in which these

catalysts are involved was not in the scope of this study. However, some of the more noticeable improvements in the production of the mentioned compounds that may be attributed to the selectivity and configuration placement phenomena are pointed out here.

Production of 4,4-dimethyl-2-pentene, and 1-ethyl-3-methyl-benzene were highest when the nickel impregnated zeolite catalysts were used. LTL and ZSM-5 zeolite catalysts significantly increased the amount of phenol in the liquid product. Highest concentrations of 1-ethyl-2-methyl-benzene were observed in the liquid products of the experiments with NiZY SS and ZSM-5 catalysts. Moreover, the production of naphthalene and 2-propyl-cyclohexanone were highest in the experiments with NiZY NS and LTL catalysts.

Some of these compounds have already found several commercial and industrial uses. For instance, diacetone alcohol is mainly used in industrial coatings, household cleaners, inks, paints, paint removers, paint thinners, pharmaceutical preparations, sealants, and pesticides [112]. Phenol has also found vast applications in industry. The major uses of phenol, consuming two thirds of its production, involve its conversion to precursors of plastics [113]. Moreover, phenol is a widely used precursor to a large collection of drugs such as aspirin, as well as many herbicides and other pharmaceuticals. Naphthalenes have applications in the production of many synthetic dyes, rubber processing chemicals, lavatory deodorant discs, wood preservatives, fungicides, and mothballs. It has also been used as an intestinal antiseptic or vermicide, as well as a low-volatility solvent [114].

### *4.2.4 Kinetics study*

Generally, the rate of an isothermal solid-state reaction is described by,

$$\mathrm{r} = \frac{\mathrm{dx}}{\mathrm{dt}} = \mathrm{k(T)}f(x) \qquad (4.1)$$

Where k(T) is the specific reaction rate or the rate constant, and f(x), known as the reaction model, is a function of x that is used to describe the system.

The rate constant k(T) is expresses by the Arrhenius equation,

$$k(T) = Ae^{-\left(\frac{Ea}{RT}\right)} \tag{4.2}$$

Where A is the pre-exponential factor or frequency factor, $E_a$ is the activation energy, T is the absolute temperature, R is the universal gas constant, x is the degree of conversion.

The degree of conversion for a solid-state isothermal reaction at any time is defined by,

$$x = \frac{m_0 - m_t}{m_0 - m_f} = \frac{(m_0 - m_{cat}) - (m_t - m_{cat})}{(m_0 - m_{cat}) - (m_f - m_{cat})} \tag{4.3}$$

Where $m_0$ is the initial mass, $m_t$ is mass at time t, $m_{cat}$ is the catalyst mass, and $m_f$ is the final mass. For non-isothermal reactions the conversion at any temperature can be defined by,

$$x = \frac{m_0 - m_T}{m_0 - m_f} = \frac{(m_0 - m_{cat}) - (m_t - m_{cat})}{(m_0 - m_{cat}) - (m_f - m_{cat})} \tag{4.4}$$

where $m_T$ is the sample weight at temperature T.

Considering the heating program of the thermogravimetric experiments in this study, sample mass at beginning of the second non-isothermal step and the end of the second isothermal steps were taken as the initial and final masses, respectively.

For each isothermal pyrolysis temperature, the rate constant can be calculated for each reaction according to the chosen reaction model. The Arrhenius parameters are consequently estimated according to the logarithmic form of the Arrhenius equation,

$$\ln k(T) = \ln A - \frac{E_a}{RT} \tag{4.5}$$

by plotting ln k(T) versus 1/T for the isothermal pyrolysis reactions at different temperatures.

Alternatively, equation (4.1) can be transformed into a new equation that describes the non-isothermal reaction rate a constant heating rate, by the following equation:

$$r = \frac{dx}{dT} = \frac{dx}{dt}\frac{dt}{dT} \tag{4.6}$$

Where, dx/dT, and dx/dt are the non-isothermal and isothermal reaction rates, respectively. In non-isothermal conditions, the constant heating rate β is defined as follows:

$$\beta = \frac{dT}{dt} \tag{4.7}$$

Successively, equation (4.8) representing the non-isothermal reaction rate can be derived.

$$r = \frac{\mathrm{d}x}{\mathrm{d}T} = \frac{A}{\beta} e^{-\left(\frac{E_a}{RT}\right)} f(x) \tag{4.8}$$

Integral method can be employed to solve this equation. The integral form for pyrolysis of boundary dam coal is as follows:

$$G(x) = \int_0^x \frac{dx}{f(x)} = \frac{A}{\beta}\int_0^T e^{-\left(\frac{E_a}{RT}\right)} dT \tag{4.9}$$

The right-hand side of equation (4.9) has analytical solution. Therefore, for the non-isothermal kinetics study, several mathematical methods have been developed to estimate the Arrhenius parameters. Coats-Redfern is one of the most popular methods that gives an approximation for the integral of the right side of the equation (4.9). The following equation has been obtained by applying the Coats-Redfern's approximation [115].

$$\ln\left[\frac{G(x)}{T^2}\right] = \ln\left(\frac{AR}{\beta E_a}\right) - \frac{E_a}{RT} \tag{4.10}$$

Consequently, the activation energy and frequency factor for a non-isothermal solid state reaction can be obtained from the slope and intercept of the $\ln[G(x)/T^2)$ vs. 1/T plot, respectively. The following kinetics model using three orders of reaction (n= 1, 2 and 3) was used throughout this study:

$$f(x) = (1-x)^n \tag{4.11}$$

Assuming different orders of reaction and substituting equation (4.11), equation (4.10) can be rewritten as follows:

$$ln\left[-\frac{\ln(1-x)}{T^2}\right] = ln\left(\frac{AR}{\beta E_a}\right) - \frac{E_a}{RT} \qquad n = 1 \tag{4.12}$$

$$ln\left[-\frac{1-(1-x)^{1-n}}{T^2(n-1)}\right] = ln\left(\frac{AR}{\beta E_a}\right) - \frac{E_a}{RT} \qquad n \neq 1 \tag{4.13}$$

Details of deriving these equations have been reported in the literature [115].

4.2.4.1 Thermogravimetric analysis (TGA) of experiments with NS type Y zeolite catalysts

Thermogravimetric curves were used to study the changes of the reaction rate during the pyrolysis reaction. Non-isothermal kinetic parameters were obtained from the plots of

$\ln[G(x)/T^2]$ versus 1/T for the boundary dam coal using 0,10 and 20 percent catalyst at a heating rate of 50K/min. Due to the similarity of the plots, only one is shown in Figure 4.26, as an example. Arrhenius parameters obtained from the TG data showed a wide variability, indicating a strong dependence on the chosen reaction mechanism. Based on the correlation coefficients, the second order reaction model was found to give the best representation of the pyrolysis reaction with $R^2$ greater than 0.99.

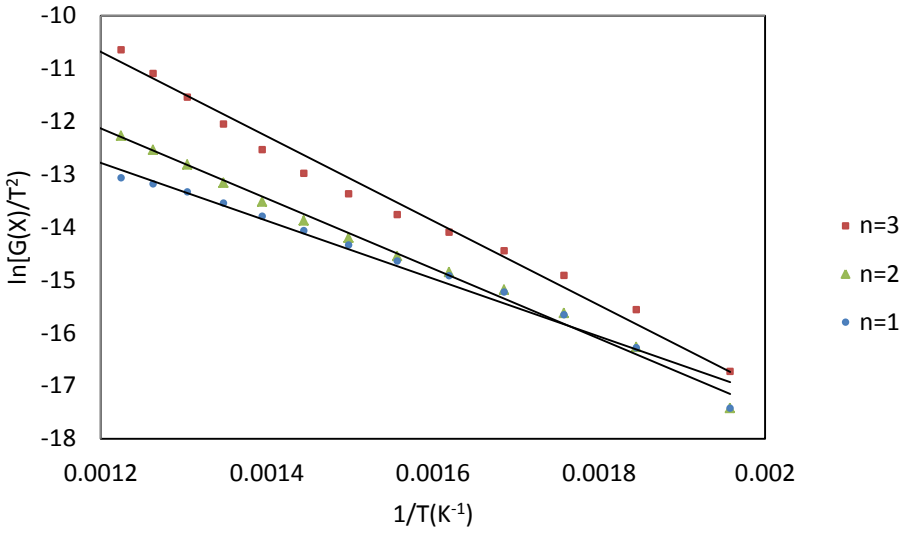


**Figure 4.26** Plot of $\ln[G(x)/T^2]$ vs. 1/T for samples with 10 percent of NaY NS catalyst

A complete set of the estimated non-isothermal kinetic parameters derived from the above-mentioned $\ln[G(x)/T^2]$ versus 1/T graphs for samples with 0, 10 and 20 percent catalyst is presented in Table 4.13.

**Table 4.13** Kinetics parameters for the non-isothermal step of the pyrolysis reactions with NS type Y catalysts

| Catalyst | Reaction order | E (kJ/mol) | A($min^{-1}$) | $R^2$ |
|---|---|---|---|---|
| None | n=1 | 45.66 | 0.60 | 0.966 |
| | n=2 | 55.32 | 5.65 | 0.990 |
| | n=3 | 66.75 | 154.02 | 0.989 |
| 10 % NaY | n=1 | 45.00 | 0.52 | 0.981 |
| | n=2 | 54.76 | 5.01 | 0.995 |
| | n=3 | 66.33 | 140.24 | 0.986 |
| 20% NaY | n=1 | 45.53 | 0.55 | 0.981 |
| | n=2 | 54.67 | 5.05 | 0.994 |
| | n=3 | 66.40 | 132.81 | 0.983 |
| 10% H-ZY | n=1 | 44.41 | 0.47 | 0.973 |
| | n=2 | 54.05 | 4.42 | 0.992 |
| | n=3 | 65.47 | 120.11 | 0.985 |
| 20% H-ZY | n=1 | 42.75 | 0.34 | 0.981 |
| | n=2 | 52.27 | 3.15 | 0.995 |
| | n=3 | 63.53 | 83.13 | 0.984 |
| 10% Ni-ZY | n=1 | 43.90 | 0.42 | 0.980 |
| | n=2 | 53.46 | 3.87 | 0.993 |
| | n=3 | 64.77 | 102.60 | 0.984 |
| 20% Ni-ZY | n=1 | 44.07 | 0.43 | 0.975 |
| | n=2 | 53.57 | 3.93 | 0.991 |
| | n=3 | 64.82 | 102.78 | 0.983 |

It can be seen that the values for the activation energies and frequency factors increase with the increase of the reaction order, but it does not show significant variations within each reaction order. As Table 4.13 indicates, the addition of the catalysts has only slightly decreased

the activation energies, which may be indicative of small catalytic activities at this stage of the reaction.

Furthermore, the second order reaction model was found to describe the isothermal stage of the reactions with $R^2$ values greater than 0.87. Consequently, the Arrhenius parameters for the isothermal step of the pyrolysis reactions were obtained using plots of Equation (4.5). The corresponding plot for the pyrolysis using the NaY NS catalyst is presented in Figure 4.27 as an example. The linearity of the ln(k) vs. 1/T diagram shows that the reaction mechanism does not change within this range of temperature. Complete results of the isothermal kinetics study based on the above-mentioned plots are presented in Table 4.14.

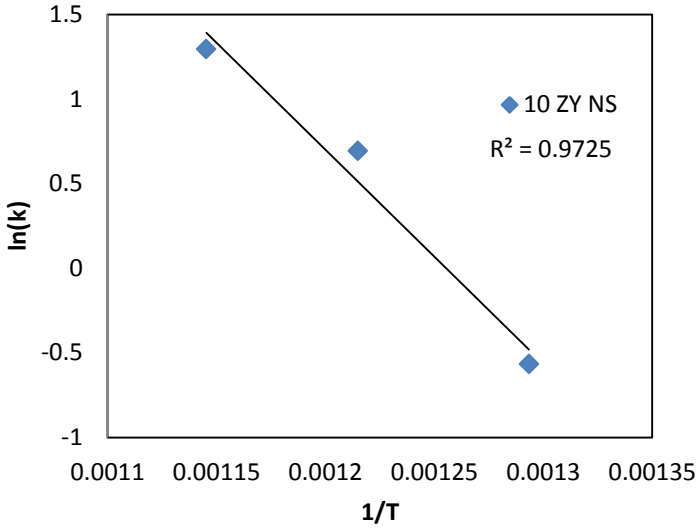


**Figure 4.27** Plot of ln(A) vs. 1/T for the samples containing 10% NaY NS

**Table 4.14** Kinetics parameters for the isothermal step of the pyrolysis reactions with NS type Y catalysts

| Catalyst Type | $E_a$ (kJ/mol) | A ($min^{-1}$) | $R^2$ |
|---|---|---|---|
| None | 151.6 | 23.0 | 0.99 |
| 10% Y NS | 105.1 | 15.9 | 0.97 |
| 20% Y NS | 102.4 | 15.8 | 0.98 |
| 10% HY NS | 111.6 | 17.0 | 0.98 |
| 20% HY NS | 107.6 | 16.2 | 0.96 |
| 10% NiY NS | 103.0 | 15.7 | 0.99 |
| 20% NiY NS | 104.1 | 15.8 | 0.98 |

The kinetic parameters obtained for the isothermal step of the reaction showed substantial variations when catalysts were added. The differences may be attributed to the unique structure, pore distributions, selectivity and acidity of the catalyst. The most significant effect on the reaction kinetics was observed when 10 % Ni-ZY NS was used. For the pyrolysis of coal, a lower energy of activation implies that the reaction needs less energy from the surroundings. Activation energy for the experiment with a coal sample containing 10 percent of this catalyst was 48kJ/mol lower than that of the experiment with the catalyst-free coal sample. However, the energy of activation obtained for the experiments with 20% catalyst were almost the same as those with 10% catalyst.

As indicated in Tables 4.13 and 4.14, notable differences exist between the values of the kinetic parameters from the isothermal and non-isothermal TG data. This may be explained by the different reactions that take place in the non-isothermal and isothermal steps, the increased

catalytic activity in the isothermal stage of the reaction due to higher temperatures, and the presence of gaseous products such as $H_2$ and $CH_4$.

4.2.4.2 Thermogravimetric analysis (TGA) of experiments with SS type Y zeolite catalysts

Similarly, the kinetics parameters were obtained for the SS type Y zeolites. These kinetics results for the non-isothermal and isothermal sections are presented in Tables 4.15 and 4.16, respectively.

**Table 4.15** Kinetics parameters for the non-isothermal step of the pyrolysis reactions with SS type Y catalysts

| Catalyst | Reaction order | E (kJ/mol) | A ($min^{-1}$) | $R^2$ |
|---|---|---|---|---|
| None | n=1 | 45.66 | 0.60 | 0.97 |
| | n=2 | 55.32 | 5.65 | 0.99 |
| | n=3 | 66.75 | 154.02 | 0.99 |
| 10 % NaY | n=1 | 45.24 | 0.54 | 0.98 |
| | n=2 | 54.96 | 5.18 | 0.99 |
| | n=3 | 66.47 | 143.09 | 0.99 |
| 20% NaY | n=1 | 44.98 | 0.51 | 0.98 |
| | n=2 | 54.69 | 4.87 | 0.99 |
| | n=3 | 66.20 | 134.21 | 0.98 |
| 10% H-ZY | n=1 | 45.16 | 0.55 | 0.97 |
| | n=2 | 55.13 | 5.64 | 0.99 |
| | n=3 | 66.97 | 168.02 | 0.99 |
| 20% H-ZY | n=1 | 42.99 | 0.36 | 0.98 |
| | n=2 | 52.26 | 3.13 | 0.99 |
| | n=3 | 63.20 | 77.31 | 0.99 |
| 10% Ni-ZY | n=1 | 45.11 | 0.53 | 0.98 |
| | n=2 | 55.01 | 5.33 | 0.99 |
| | n=3 | 66.76 | 155.33 | 0.99 |
| 20% Ni-ZY | n=1 | 43.68 | 0.39 | 0.98 |
| | n=2 | 53.07 | 3.53 | 0.99 |
| | n=3 | 64.17 | 89.36 | 0.98 |

The kinetics parameters of the non-isothermal stage obtained for the SS type Y catalysts were very similar to those of NS type catalysts and showed similar trends. Moreover, the energies of activation for the experiments with catalyst are only slightly different from the

activation energies of the experiments without catalyst, which may, similar to the experiments with NS type catalysts, suggest insignificant catalytic effect at this stage of the reaction.

**Table 4.16** Kinetics parameters for the isothermal step of the pyrolysis reactions with SS type Y catalysts

| Catalyst | $E_a$ (kJ/mol) | Ln(A) | $R^2$ |
|---|---|---|---|
| None | 151.6 | 23.1 | 0.99 |
| 10 % NaY | 115.9 | 17.1 | 0.98 |
| 20% NaY | 113.1 | 17.3 | 0.98 |
| 10% H-ZY | 97.1 | 14.8 | 0.98 |
| 20% H-ZY | 96.8 | 15.1 | 0.98 |
| 10% Ni-ZY | 122.3 | 18.6 | 0.99 |
| 20% Ni-ZY | 125.8 | 19.2 | 0.98 |

The activation energies observed for the experiments with the SS type Y catalysts showed some differences from those of NS type Y catalysts. Since the NS and SS type Y zeolites have similar structures, the differences can be attributed to the different SARs and the surface areas of these zeolites. Moreover, the degree of completeness of the ion exchange processes and possible structural damages introduced to the zeolite frameworks due to the post-secondary treatments may have also affected the results. Experiments with sodium and nickel oxide impregnated SS type Y catalysts had higher activation energies than those of NS type Y catalysts, while the hydrogen form SS type catalysts had lower activation energies than those of hydrogen form NS type catalysts. The differences observed for the sodium form catalysts are

most likely due to the SAR ratio, whereas for the modified forms, the effectiveness of the post-secondary treatments also influences the results.

4.2.4.3 Thermogravimetric analysis (TGA) of experiments with ZSM-5 zeolite catalysts

The kinetics parameters obtained for the experiments with ZSM-5 zeolites are presented in Tables 4.17 and 4.18.

**Table 4.17** Kinetics parameters for the non-isothermal step of the pyrolysis reactions with ZSM-5 catalysts

| Catalyst | Reaction order | E (kJ/mol) | A ($min^{-1}$) | $R^2$ |
|---|---|---|---|---|
| None | n=1 | 45.66 | 0.60 | 0.97 |
| | n=2 | 55.32 | 5.65 | 0.99 |
| | n=3 | 66.75 | 154.02 | 0.99 |
| 10 % ZSM-5 | n=1 | 44.55 | 0.48 | 0.98 |
| | n=2 | 54.13 | 4.48 | 0.99 |
| | n=3 | 65.45 | 119.54 | 0.99 |
| 20 % ZSM-5 | n=1 | 43.23 | 0.37 | 0.98 |
| | n=2 | 52.65 | 3.34 | 1.00 |
| | n=3 | 63.76 | 85.38 | 0.99 |
| 10 % HZSM-5 | n=1 | 45.60 | 0.61 | 0.98 |
| | n=2 | 56.00 | 6.84 | 1.00 |
| | n=3 | 68.38 | 229.09 | 0.99 |
| 20% HZSM-5 | n=1 | 44.23 | 0.45 | 0.98 |
| | n=2 | 53.74 | 4.13 | 0.99 |
| | n=3 | 64.97 | 108.27 | 0.99 |

**Table 4.18** Kinetics parameters for the isothermal step of the pyrolysis reactions with ZSM-5 catalysts

| Catalyst | $E_a$ (kJ/mol) | ln(A) | $R^2$ |
|---|---|---|---|
| None | 151.6 | 23.0 | 0.99 |
| 10 % ZSM-5 | 104.4 | 15.8 | 0.98 |
| 20 % ZSM-5 | 101.3 | 15.3 | 0.98 |
| 10 % HZSM-5 | 115.8 | 17.5 | 0.97 |
| 20% HZSM-5 | 111.5 | 16.8 | 0.99 |

In both non-isothermal and isothermal stages of the experiments with ZSM-5 type catalysts, similar changes to those of type Y catalysts were observed. Although the properties of ZSM-5 zeolites are remarkably different from those of type Y zeolites, no significant differences were observed in the results of the kinetics study of the experiments with these catalysts.

4.2.4.3.1 Thermogravimetric analysis (TGA) of experiments with LTL zeolite catalysts

The kinetics parameters obtained for the experiments with LTL zeolites are presented in Tables 4.19 and 4.20.

**Table 4.19** Kinetics parameters for the non-isothermal step of the pyrolysis reactions with LTL catalysts

| Catalyst | Reaction order | E (kJ/mol) | A($min^{-1}$) | $R^2$ |
|---|---|---|---|---|
| None | n=1 | 45.66 | 0.60 | 0.97 |
| | n=2 | 55.32 | 5.65 | 0.99 |
| | n=3 | 66.75 | 154.02 | 0.99 |
| 10 % LTL | n=1 | 45.20 | 0.55 | 0.98 |
| | n=2 | 55.12 | 5.50 | 0.99 |
| | n=3 | 66.88 | 160.71 | 0.99 |
| 20 % LTL | n=1 | 45.93 | 0.65 | 0.98 |
| | n=2 | 56.23 | 7.06 | 1.00 |
| | n=3 | 68.49 | 230.06 | 0.99 |
| 10 % HLTL | n=1 | 45.26 | 0.55 | 0.98 |
| | n=2 | 55.04 | 5.39 | 0.99 |
| | n=3 | 66.63 | 151.94 | 0.99 |
| 20% H-ZY | n=1 | 44.23 | 0.45 | 0.98 |
| | n=2 | 53.74 | 4.13 | 0.99 |
| | n=3 | 64.97 | 108.27 | 0.99 |

**Table 4.20** Kinetics parameters for the isothermal step of the pyrolysis reactions with LTL catalysts

| Catalyst | $E_a$(kJ/mol) | A($min^{-1}$) | $R^2$ |
|---|---|---|---|
| None | 151.6 | 23.0 | 0.99 |
| 10 % LTL | 129.3 | 19.7 | 0.96 |
| 20% LTL | 133.6 | 18.6 | 0.99 |
| 10% H-LTL | 105.0 | 16.0 | 0.97 |
| 20% H-LTL | 106.8 | 16.21 | 0.98 |

The kinetics study of the catalytic coal pyrolysis experiments showed significant reductions in the values of the activation energy due to the presence of catalysts. However, the reductions caused by the presence of different types of zeolite catalysts were similar to each other.

# Chapter Five: **Conclusions**

Direct hydrothermal synthesis of LTY, ZSM-5 and LTL type zeolites, without the use of organic structure directing agents was successfully carried out. Pure zeolite Y, using sodium silicate as the silicon source, with low solubility and reactivity and without the use of any organic SDAs or seeding gel, can be synthesized via a direct hydrothermal method from the starting gel composition of $5.35Na_2O:1Al_2O_3:3.83SiO_2:154H_2O$. This new starting gel composition made it possible to obtain pure crystalline zeolite Y with high crystallinity, surface area, and thermal stability. The samples fabricated from this silicon source presented comparable properties with those prepared from conventional colloidal silica, in terms of ion-exchange ability, SAR, particle size, and specific surface area. Template-free synthesis of ZSM-5 and LTL zeolites was found to be possible using the new starting gel compositions of $7.15Na_2O:1Al_2O_3:47.61SiO_2:1190H_2O$ and $10K_2O:60SiO_2:1Al_2O_3:400H_2O$, respectively.

Various modification techniques were applied to obtain the modified zeolites, and the effects of the modifications on the zeolite powders were investigated. All zeolites were successfully modified by ion exchange and thermal treatments and were shown to properly retain their characteristics. It was shown that regardless of the type of silicon source used, type Y zeolites could be impregnated with nickel oxide by adding a nickel-containing solution to the synthesis starting gel right before the hydrothermal stage, followed by calcination. The resultant impregnated zeolites prepared by this method also demonstrated high crystallinity and surface area.

Application of these zeolites in pyrolysis of the Saskatchewan boundary dam coal influenced the products of the pyrolysis reaction and improved the amounts of a number of valuable compounds, such as phenol, while leaving a carbon-rich solid residue.

It was found that ZSM-5 and LTL type zeolite catalysts can increase the production of phenol. Most significantly, phenol was increased up to around 50% in the liquid product obtained using the H-LTL zeolite catalyst.

Kinetics studies showed that these catalysts significantly reduced the activation energies of the coal pyrolysis reactions. However, different catalyst types performed differently.

## 5.1 Recommendations

In this study zeolite catalysts were completely mixed with the coal to gain maximum contact. However, zeolite catalysts can be recovered through thermal treatment and washing. Moreover, zeolites can be shaped into granular beads or palettes to facilitate the process of separating the catalysts.

Presented below are some recommendations for future research in the area of catalytic coal pyrolysis using zeolite catalysts.

1. Development of new conditions to synthesize zeolite Y using sodium silicate with higher Si/Al ratio.
2. Examination of the effect of temperature on the template free synthesis of ZSM-5 zeolites with the aim to eliminate the impurity phases.
3. Establishment of methods for synthesis of zeolites in a continuous system.
4. Shaping zeolites, and utilizing shaped zeolite catalysts in pyrolysis reactions in separate beds, in order to facilitate catalyst regeneration.
5. More comprehensive measurement of produced gasses including C2-C5 and sulfur-containing gasses.

Investigation of other potential uses of zeolitic materials for further improvement of the pyrolysis reaction, such as pollution control (use of zeolites as molecular sieves).

**References**


1. **C. Colella, A.F. Gualtieri.** *Cronstedt's zeolite*, Microporous and Mesoporous Materials, **2007**, Vol. 105, 213-221.

2. **R.M. Barrer.** *Hydrothermal Chemistry of Zeolites*, London : Academic Press, **1982**.

3. **R. M. Barrer, C. Marcilly.** *Hydrothermal chemistry of silicates. Part XV. Synthesis and nature of some salt-bearing aluminosilicates.* Journal of Chemical Society, **1970,** 2735-2745.

4. **J. (Editor), A. Corma (Editor), S. Zones (Editor).** *Zeolites and Catalysis: Synthesis, Reactions and Applications*, Wiley-VCH, **2010**.

5. **E.M. Flanigen, J.C. Jansen, H. Bekkum.** *Introduction to Zeolite Science and Practice.* Elsevier, **2007**.

6. **M. Danilczuk, K Długopolska, T Ruman, D Pogocki.** *Molecular sieves in medicine.* Mini-Reviews in Medicinal Chemistry, **2008,** Vol 13, 1407-1417.

7. **H. Oguz, V. Kurtoglu.** *Effect of clinoptilolite on performance of broiler chickens during experimental aflatoxicosis*, British Poultry Science, **2000, Vol 41**, 512-517.

8. **Walter Meier, David H. Olson, Ch Baerlocher.** *Atlas of Zeolite Structure Types., International Zeolite Association Structure Commission.* **2007.**

9. **S.H. Lin, M. Harada, Y. Suzuki, H. Hatano.** *Comparison of pyrolysis production between coal, coal/CaO, and coal/Ca(OH)$_2$ materials.* Energy & Fuels, **2003**, *Vol 17.*

10. **C.S. Wen, T.P. Kobylinski.** *The Chemistry of Low-RankCoals.* American Chemical Society, Washington DC, **1984,** Vol. 264.

11. **M. Chareonpanich, T. Boonfueng, J. Limtrakul.** P*roduction of aromatic hydro-carbons from Mae-Moh lignite* . Fuel Processing Technology , **2002**, Vol 79, 171‑179.

12. **T. Isoda, K. Kusakabe, and Sh. Morooka, I. Mochida.** *Reactivity and selectivity for the hydrocracking of vacuum gas oil over metal-loaded and dealuminated Y-zeolites.* Enery and Fuels, **1998,** Vol. 12, 493-502.

13. **Dekker, Macel.** *Handbook of zeolite science and technology.* New York, **2003**.

14. **N.R.Shijua, V.V. Guliants.** *Recent developments in catalysis using nanostructured materials.*, Applied Catalysis, **2009**, Vol. 356, 1-17.

15. **Sh. Wang, U. Peng.** *Natural zeolites as effective adsorbents in water and wastewater treatment.*, Chemical Engineering Journal, **2010**, Vol. 156, 11-24.

16. **A. Aho, N. Kumar, K, Eraenen, T. Salmi, M. Hupta, D.Y. Murzin.** *Catalytic Pyrolysis of woody biomass in a fluidized bed reactor: influence of the zeolite structure.* Fuel, **2008**, Vol. 87. 2493-2501.

17. **L. Tosheva, V.P. Valtchev.** *Nanozeolites: synthesis, crystallization mechanism and application.*, Chemistry of materials, **2005**, Vol. 17. 2494–2513.

18. **D.W. Breck.** *Zeolite molecular sieves.* New York, Wiley, **1974**.

19. **Schuring, D.** *Diffiussion in Zeolites: Towards a microscopic understanding, MSc thesis.* Eindhoven : Eindhoven University of Technology, **2002**.

20. **P.A. Jacobs, J.A. Martens.** *Synthesis of high silica aluminosilicate zeolites.* Amsterdam : Elsevier, **1987**.

21. **M. E. Davis, R. F. Lobo.** *Zeolite and molecular sieve synthesis.* Chemistry of Materials, **1992,** Vol. 4, 756–768.

22. **S. Bhatia.** *Zeolite catalysis: Principles and applications.* CRC press, **1989**.

23. **J. Wang, L. Gao.** *Photoluminescence Properties of Nanocrystalline ZnO Ceramics Prepared by Pressureless Sintering and Spark Plasma Sintering.*, Journal of American Ceramic Society, **2005**, Vol. 88. 1637-1639.

24. **B. Elvers, S. Hawkins.** *Ullmann's Encycolopedia of Industrial Chemistry.* Weinheim : VCH Verlagsgesellschaft GmBH, **1996**, Vol. 28.

25. **R.M. Barrer.** *Syntheses and reactions of mordenite.* Journal of Chemical Society, **1948**.

26. **R. M. Barrer, L. Hinds, E. A. White.** *The hydrothermal chemistry of silicates. Part III. Reactions of analcite and leucite.* Journal of Chemical Society, **1953**. 1466-1475.

27. **R.M. Milton.** *Molecular sieve adsorbents, 2882243* US Patent, **1959**.

28. **R.M. Milton.** *Molecular sieve adsorbents, 2882244* US Patent, **1959**.

29. **R. M. Milton.** *Molecular Sieve Science and Technology.* American Chemical Society, **1989**.

30. **R.J. Argauer, G.R. Landolt.** *Crystalline zeolite zsm-5 and method of preparing the same, 3702886* US Patent, **1972**.

31. **S. M. Auerbach, K. A. Carrado, P. K. Dutta.** *Handbook of zeolite science and technology.* New York : CRC Press, **2003**.

32. **L. B. McCusker, F. Liebau, G. Engelhardt.** *Nomenclature of structural and compositional characteristics of ordered microporous and mesoporous materials with inorganic hosts.* Pure Applied Chemistry, **2001**, Vol. 73, 381–394.

33. **R. M. Barrer.** *Clay minerals as selective and shape-selective sorbents.* Pure Applied Chemistry, **1989**, Vol. 61, 1903-1912.

34. **Q. Zhou, Y. Wang, Ch. Tang, Y. Zhang.** *Modifications of ZSM-5 zeolites and their applications in catalytic degradation of LDPE.* Polymer Degradation and Stability, **2003**, Vol. 80, 23-30.

35. **H. Villiger, R.M. Barrer.** *The Crystal Structure of the Synthetic Zeolite L. Z.* Kristallogeom, Kristallphys. Kristalchem, **1969**, Vol. 128, 352-370.

36. **R.M. Barrer, Ch. Baerlocher.** *The structure of the synthetic zeolite (K Ba)-G, L, Z.* Kristallogr. Kristallgeom. Kristallphys. Kristallchem, **1972**, Vol. 136, 245-254.

37. **J.M. Newsam.** *Structural Characterization of Dehydrated Gallium Zeolite L.* Materials Research Bulletin, **1986**, Vol. 21, 661-672.

38. **S. Zone, M.E. Davis.** *Zeolite materials: recent discoveries and future prospects. Current Opinion in Solid State and Materials Science*, **1996**, Vol. 1, 107-117.

39. **A. Corma.** *From Microporous to Mesoporous Molecular Sieve Materials and Their Use in Catalysis.* Chemical Reviews, **1997**, Vol. 97, 2373-2420.

40. **D. Bruehwiler, G. Calzaferri.** *Molecular sieves as host materials for supramolecular organization.* Microporous and Mesoporous Materials, **2004**, Vol. 72, 1-23.

41. **M. Yoshimura, K. Byrappa.** *Handbook of Hydrothermal Technology.* New Jersey: Noyes Publications, **2001**.

42. **A. Rabenau.** *The Role of Hydrothermal Synthesis in Preparative Chemistry.* Angewandte Chemie International Edition in English, **1985**, Vol. 24, 1026-1040.

43. **M. Czjzek, H. Jobic, A. N. Fitch, T. Vogt.** *Direct determination of proton positions in D-Y and H-Y zeolite samples by neutron powder diffraction.* Pysical Chemistry, **1992**, Vol. 4. 1535–1540.

44. **P.A.Wright.** *Microporous framework solids.* Cambridge : RSC Publishing, **2008**. 978-0-85404-812-0.

45. **G. Brunner.** *Near and supercritical water. Part II: Oxidative processes.* The journal of supercritical fluids, **2009**, Vol. 47, 382-390.

46. **J.F. Yao, L. Yu, L.X. Zhang, H.T. Wang.** *Influence of glycerol cosolvent on the synthesis.* Materials Letters, **2011,** Vol. 65, 2304‑2306.

47.**J. Perez-Ramirez, C.H. Christensen, K. Egeblad, J.C. Groen.** *Hierarchical zeolites:enhanced utilisation of microporous crystals in catalysis by advances in materials design.* Chemical Society Reviews, **2008,** Vol. 37, 2530-2542.

48. **I. Krznaric, T. Antonic, J. Bronic, B. Subotic, R.W. Thompson.** *Influence of silica sources on the chemical composition of aluminosilicate hydrogels and the results of their hydrothermal treatment.* Croatica Chemica Acta, **2003,** Vol. 76, 7-17.

49. **B. Bayati, A.A. Babaluo, R. Karimi.** *Hydrothermal synthesis of nanostructure NaA zeolite: the effect of synthesis parameters on zeolite seed size and crystallinity.* Journal of the European Ceramic Society, **2008,** Vol. 28, 2653‑2657.

50. **S. Bosnar, J. Bronic, I. Krznaric, B. Subotic.** *Influence of concentrations of aluminium and silicon in the liquid phase on the growth kinetics of zeolite A and X microcrystals.* Croatica Chemica Acta, **2005,** Vol. 78, 1-8.

51. **C. Berger, R. Glaser, R.A. Rakoczy, J. Weitkamp.** *The synthesis of large crystals of zeolite Y re-visited.* Microporous and Mesoporous Materials, **2005,** Vol. 83, 333-344.

52. **R. M. Mohamed, Hisham M. Aly, M. F. El-Shahat, I. A. Ibrahim.** *Effect of the silica sources on the crystallinity of nanosized ZSM-5 zeolite.* Microporous and mesoporous materials, **2004**, Vol. 79, 7-12.

53. **B. Lu, T. Tsuda, H. Sasaki, Y. Oumi, K. Itabashi, T. Teranishi, T. Sano.** *Effect of Aluminum Source on Hydrothermal Synthesis of High-Silica Mordenite in Fluoride Medium, and It's Thermal Stability.* Chemistery of Materials, **2004,** Vol. 16, 286-291.

54. **A. Charkhi, H. Kazemian, M. Kazemeini.** *Optimized experimental design for natural clinoptilolite zeolite ball milling to produce nano powders.* Power Technology, **2010,** Vol 203, 389-396.

55. **B. A. Holmberg, H. Wang, J. M. Norbeck, Y. Yan.** *Controlling size and yield of zeolite Y nanocrystals using tetramethylammonium bromide.* Microporous and mesoporous materials, **2003**, Vol. 59, 13-28.

56. **B.M. Lok, T.R. Cannan, C.A. Messina.** *The role of organic molecules in molecular sieve synthesis.* Zeolites, **1983**, Vol. 3, 282-291.

57. **S. Ferchiche, J. Warzywoda, A. Sacco Jr.** *Direct synthesis of zeolite Y with large particle size.* International Journal of Inorganic Materials, **2001,** Vol. 3, 773-780.

58. **J. Bronić, B. Subotić, I. Smit, L.J.A. Despotović.** *Influence of Gel Ageing on Zeolite Nucleation Processes.* Studies in Surface Science and Catalysis, **1988**, Vol. 37, 107-114.

59. **M. Ogura, Y. Kawazu, H. Takahash , T. Okubo.** *Aluminosilicate Species in the Hydrogel Phase Formed during the Aging Process for the Crystallization of FAU Zeolite.* Chemistry of Materials, **2003**, Vol. 15, 2661-2667.

60. **H. Kacirek, H. Lechert.** *Rates of crystallization and a model for the growth of sodium-Y zeolites.* The Journal of Physical Chemistry, **1976**, Vol. 80, 1291-1296.

61. **J. Ciric.** *Kinetics of zeolite A crystallization.* Journal of Colloid and Interface Science, **1968**, Vol. 28, 315-324.

62. **S.P. Zhdanov, N.N. Feoktistova, L.M. Vtjurina.** *Temperature Dependence of Nucleation of Zeolites in Alkaline Aluminosilicate Gels In Hydrothermal Crystallization Conditions,* Studies in Surface Science and Catalysis, **1991**, Vol. 65, 287-296.

63. **C. S. Cundy, B. M. Lowe, D. M. Sinclair.***Crystallisation of zeolitic molecular sieves: direct measurements of the growth behaviour of single crystals as a function of synthesis conditions.* Faraday discussions, 1993, Vol. 95, 235-252.

64. **P. Massiani, F. Fajula, F. Renzo, F. Remoue, F. Figueras.** *The Influence of History Dependent Factors on the Properties of Zeolite Catalysts.* Studies in Surface Science and Catalysis, **1989**, Vol. 52, 215-225.

65. **P.S. Wheatley, A.R. Butler, M.S. Crane, A.G. Rossi, I.L. Megson, R.E. Morris.** *Zeolites for storage and delivery of nitric oxide in human physiology.* Studies in Surface Science and Catalysis, **2005**, Vol. 158, 2033-2040.

66. **Weitkamp, Jens.** *Zeolites and Catalysis.* Solid State Ionics, **2000**, Vol. 131.

67. **G. Centia, P. Ciambelli, S. Perathoner, P. Russo.** *Environmental catalysis: trends and outlook.* Catalysis Today, **2002**, Vol. 75, 3-15.

68. **C.R. Marcilly.** *Where and how shape selectivity of molecular sieves operates in refining and petrochemistry catalytic processes.* Topics in Catalysis, **2000**, Vol. 13, 357-366.

69. **C. J. Plank, E. J. Rosinski , W. P. Hawthorne.** *Acidic Crystalline Aluminosilicates. New Superactive, Superselective Cracking Catalysts.* Industrial & Engineering Chemistry Research, **1964**, Vol. 3, 165-169.

70. **P. R. Solomon, T. H. Fletcher, R. J. Pugmire.** *Progress in coal pyrolysis.* Advanced Fuel Research, **1992,** Vol. 72,69-73.

71. **T.Green, J.Kovac, D.Brenner, J.Larsen.** *Coal Structure.* New York : Academic Press, **1982**.

72. **L. Cui, W.Lin,J. Yao.** *Influences of temperature and coal particle size on the flash pyrolysis of coal in a fast-entrained bed.* Chemical Research in Chinese Universities, **2006**, Vol. 22. 103-110.

73. **N. Qui, H. Li, Z. Jin, Y. Zhu.** *Temperature and time effect on the concentrations of free radicals in coal: evidence from laboratory pyrolysis experiments.* International Journal of Coal Geology, **2007**, Vol. 69. 220-228.

74. **M.D. Casal, C.S. Canga, M.A. Diez.** *Low temperature pyrolysis of coals with different coking pressure characteristics.* Journal of Analytical and Applied Pyrolysis, **2005**, Vol. 74, 96-103.

75. **L.P. Wiktorsson, W. Wanzel.** *Kinetic parameters for coal pyrolysis at low and high heating rates- A comparison of data from different laboratory equipment.* Fuel, **2000**, Vol. 79, 701-716.

76. **A.G. Shalimov.** *Corex process for making high-quality steels at mini-mills.* Metallurgy, **2002**, Vol. 44.

77. **D.W.Van. Krevelen.***Coal: Topology-Chemistry-Physics-Constitution.* Amsterdam: Elsevier, **1961**.

78. **A.W. Scaroni, M.Rashid Khan Usdoe, S. Eser, L.R. Radovic.** *Coal Pyrolysis.* Ullmann's encyclopedia of industrial chemistry, **2011**.

79. **W.Kamisky.** *Thermal recycling of polymers.* Journal of Analitical and Applied Pyrolysis, **1985,** Vol. 3, 1543-1552.

80. **P.T. Williams, P.A. Home, D.T. Taylor.** *Polycyclic aromatic hydrocarbons in polystyrene derived pyrolysis oil.* Journal of Analytical and Applied Pyrolysis, **1993,** Vol. 25, 325-334.

81. **S. Ma, J. Hill, S. Heng.** *A kinetic analysis of the pyrolysis of some Australian coals by non-isothermal thermogravimetry.* Journal of thermal analysis, **1991**, Vol. 37. 1161-77.

82. **F. Fraga, E.R. Nunez.** *Activation energy for the epoxy system BADGE n=0/m-XDA obtained using data from thermogravimetric analysis.* Journal of applied polymer science, **2001**, Vol. 80. 776-82.

83. **J.Y. Lee, M.J. Shim, S.W. Kim.** *Thermal decomposition kinetics of an epoxy resin with rubber-modified curing agent.* Journal of applied polymer science, **2001**, Vol. 81. 479-85.

84. **D. Karami, S. Rohani.** *A Novel Approach for the Synthesis of Zeolite Y.* Industrial and engineering chemistry research, **2009**. 4837-4843.

85. **F.J. van Der Gaag, J.C. Jansen, H. van Bekkum.** *Template Variation in the Synthesis of Zeolite ZSM-5.* Studies in Surface Science and Catalysis, **1985**, Vol. 24, 81-88.

86. **S. Mintova, V. Valtchev, E. Vulcheva, S. Veleva.** *Kinetics of zeolite ZSM-5 crystallization; template effect of propyl-substituted amines.* Materials Research Bulletin, **1992**, Vol. 27, 515-522.

87. **ER Geus, H van Bekkum.** *Calcination of large MFI-type single crystals, Part 2: Crack formation and thermomechanical properties in view of the preparation of zeolite membranes.* Zeolites, **1994**, Vol. 15, 333-341.

88. **R.Xu, W. Pang, J. Yu, Q. Huo, J. Chen.** *Chemistry of zeolites and related porous materials: synthesis and strucuture.* Singapore : John Wiley and sons, **2007**. 978-0-470-82233-3.

89. **J.H. Zou, Z.J. Zhou, F.C. Wang, W. Zhang, Z.H. Dai, H.F. Liu, Z.H. Yu.** *Modeling reaction kinetics of petroleum coke gasification with CO2.* Shanghai : Chemical Engineering and Processing, **2006**, Vol. 46, 630-636.

90. **M.M.J. Treacy, J.B. Higgins.** *Collection of Simulated XRD Powder Patterns for Zeolites.* Elsevier Published on behalf of the Stucture Commision of the International Zeolite Association, **2001**.

91. **N.E. Ghermani, C. Lecomte, Y Dusausoy.** *Electrostatic properties in zeolite-type materials from high-resolution x-ray diffraction: The case of natrolite.* Physical Review B, **1995,** Vol. 53, 5231-5239.

92. **J.D. Hanawalt, H.W. Rinn, L.K. Frevel.** *Chemical Analysis by X-Ray Diffraction.* Industrial and Engineering Chemistry, **1938**, Vol. 10, 457-512.

93. **S.B. Kulkarni, V.P. Shiralkar, A.N. Kotashane, R.B. Borade, P. Ratnasamy.** *Studies in the synthesis of ZSM-5 zeolites.* Zeolites, **1982**, Vol. 2, 313-318.

94. **E. M. Flanigen, H. Khatami, H.A. Szymanski.** Infrared Structural Studies of Zeolite Frameworks. *Zeolite Molecular Sieves.* Advances in Chemistry, **1971, Vol. 101, 201-229**.

95. **E.M. Flanigen, L.B. Sand.** *Molecular Sieve Zeolites- I.* Washington : American Chemical Society, **1971**.

96. **J. Scherzer, J. L. Bass.** *Infrared spectra of Ultrastable zeolites derived from type y zeolties.* Journal of Catalysis, **1972,** Vol. 28, 101-115.

97. **K. Byrappa, B.V Suresh Kumar.** *Characterization of Zeolites by Infrared Spectroscopy.* Asian Journal of Chemistry, **2007**, Vol. 19, 4933-4935.

98. **P. Pichat, C. Franco-Parra, D. Barthomeuf.** *Infra-red structural study of various type L zeolites.* Journal of the Chemical Society, Faraday Transactions 1: Physical Chemistry in Condensed Phases, **1975**, Vol. 71, 991-996.

99. **S. Özvatan, Y. YÜrÜm.** *Synthesis of Crystalline ZSM-5 Type Zeolites Utilizing Primary Monoalkylamines 1.Characterization.* Energy Sources, **2010,** Vol. 23, 475-485.

100. **J. Jiao, W. Wang, B. Sulikowski, J. Weitkamp, M. Hunger.** *$^{29}$Si and $^{27}$Al MAS NMR characterization of non-hydrated zeolites Y upon adsorption of ammonia.* Microporous and mesoporous materials, **2006**, Vol. 90, 246-250.

101. **J. Rocha, J. Klinowski.** *$^{27}$Al solid-state NMR spectra of ultrastable zeolite Y with fast magnetic-angle spinning and $^{27}$Al coss-polarization.* Journal of the Chemical Society, Chemical Communications, **1991,** Vol 16, 1972-1995.

102. **L. Zhang, S. Liu, S. Xie, L. Xu.** *Organic template-free synthesis of ZSM-s/ZSM-11 co-crysalline zeolite.* Microporous and Mesoporous Materials, **2011**, Vol. 147, 117-126.

103. **S. Niksa.** *Flash chain theory for rapid coal devolatilization kinetics. Predicting the release of oxygen species from various coals.* Energy Fuels, **1996**, Vol. 10,173-187.

104. **W.E. Ladner.** *The products of coal pyrolysis: properties, convertion and reactivity.* Fuel processing technology, **1988**, Vol. 20, 207-222.

105. **A. Arenillas, F.Rubiera, J.J. Pis.** *Simultaneous thermogravimetirc-mass spectrometric study on the pyrolysis behavious of different rank coals.* Journal of Analytical and Applied Pyrolysis, **1999**, Vol. 50, 31-46.

106. **L. Tao, G.B. Zhao, J. Qian, Y.K Qin.** *TG-FTIR characterization of pyrolysis of waste mixtures of paint and tar slag.* Journal of Hazardous Materials, **2010**, Vol. 175, 754-761.

107. **P.R. Solomon, D.G. Hamblen, R.H. Sclosberg (Editor).** *Chemistry of coal conversion.* New York, **1985**.

108. **P.R. Solomon, D.G. Hamblen, M.A. Serio, Z.Z. Yu, S.Charpenay.** *A characterization method and model for predicting coal conversion behavior.* Fuel, **1993**, Vol. 72, 469-488.

109. **C. Li, K. Suzuki.** *Tar property, analysis, reforming mechanism and model for biomass gasification—An overview.* Renewable & sustainable energy reviews, **2009**, Vol. 13, 594-604.

110. **Masel, R.J.** *Chemical Kinetics and Catalysis.* New York : Wiley, **2001**.

111. **Fogler, H.S.** *Elements of Chemical Reaction Engineering.* Prentice Hall, **2005**.

112. **Johann Haltermann Ltd**. Technical Data & Safety Bulletin, Diacetone Alcohol. **2012**.

113. **M. Weber, M. Kleine-Boymann.** Phenols. *Ullmann's Encyclopedia of Industrial Chemistry.* Wiley, **2004**.

114. **G. Collin, H. Höke, H. Greim.** Naphthalene and Hydronaphthalenes. *Ullmann's Encyclopedia of Industrial Chemistry.* Wiley, **2004**.

115. **A.W. Coats, J.P Redfern.** *Kinetic parameteres from thermogravimetric data.* Nature, **1964**, Vol. 201,68-69.

**Appendix A:** Some sources of error in thermogravimetric experiments and analysis

Errors in thermogravimetry analysis can result in considerable inaccuracies in the thermogravimetric analysis results. Some of the possible sources of error which can affect the thermogravimetric analysis are mentioned below.

1. Buoyancy effect
2. Condensation on balance suspension
3. Random fluctuation of balance mechanism
4. Turbulence effect from gas flow

By heating an empty thermally inert crucible, usually an apparent weight change is observed as temperature increases. This is due to effect of change in buoyancy of the gas in the sample environment with the temperature, the increased convection and possible effect of heat from the furnace on the balance itself. In most modern thermobalances, similar to the one used in this study, this effect is negligible. However, in this study, the effect of buoyancy on the sample crucible was investigated by carrying out a black run test. It was found that heating the empty crucible at a heating rate of 50K/min up to the desired final pyrolysis temperatures in nitrogen atmosphere only lead to maximum weight fluctuations of ±0.015mg, and the simultaneous recording of the gas flow rates by the thermogravimetric analyzer did not indicate any notable fluctuations in the flow rates.

Furthermore, given the accuracy and design of the thermogravimetric analyzer, and the used gas flow rates, condensation on the balance and turbulence effect from gas flow could also be disregarded.